Graduate School ETD Form 9
(Revised 12/07)

PURDUE UNIVERSITY
GRADUATE SCHOOL
Thesis/Dissertation Acceptance

This is to certify that the thesis/dissertation prepared

By JASMIN DHIRAJLAL RADADIA

Entitled A HIGHLY PRECISE AND LINEAR IC FOR HEAT PULSE BASED THERMAL BIDIRECTIONAL MASS FLOW SENSOR

For the degree of Master of Science in Electrical and Computer Engineering

Is approved by the final examining committee:

Maher E. Rizkalla
Chair

Yaobin Chen

Lingxi Li

To the best of my knowledge and as understood by the student in the *Research Integrity and Copyright Disclaimer (Graduate School Form 20)*, this thesis/dissertation adheres to the provisions of Purdue University's "Policy on Integrity in Research" and the use of copyrighted material.

Approved by Major Professor(s): Maher E. Rizkalla

Approved by: Yaobin Chen 04/26/2010
Head of the Graduate Program Date

Graduate School Form 20
(Revised 1/10)

PURDUE UNIVERSITY
GRADUATE SCHOOL

Research Integrity and Copyright Disclaimer

Title of Thesis/Dissertation:

A HIGHLY PRECISE AND LINEAR IC FOR HEAT PULSE BASED THERMAL BIDIRECTIONAL MASS FLOW SENSOR

For the degree of Master of Science in Electrical and Computer Engineering

I certify that in the preparation of this thesis, I have observed the provisions of *Purdue University Teaching, Research, and Outreach Policy on Research Misconduct (VIII.3.1)*, October 1, 2008.*

Further, I certify that this work is free of plagiarism and all materials appearing in this thesis/dissertation have been properly quoted and attributed.

I certify that all copyrighted material incorporated into this thesis/dissertation is in compliance with the United States' copyright law and that I have received written permission from the copyright owners for my use of their work, which is beyond the scope of the law. I agree to indemnify and save harmless Purdue University from any and all claims that may be asserted or that may arise from any copyright violation.

JASMIN DHIRAJLAL RADADIA

Printed Name and Signature of Candidate

04/27/2010

Date (month/day/year)

*Located at http://www.purdue.edu/policies/pages/teach_res_outreach/viii_3_1.html

A HIGHLY PRECISE AND LINEAR IC FOR HEAT PULSE BASED THERMAL BIDIRECTIONAL MASS FLOW SENSOR

A Thesis
Submitted to the Faculty
of
Purdue University
by
Jasmin Dhirajlal Radadia

In Partial Fulfillment of the
Requirements for the Degree
of
Master of Science in Electrical and Computer Engineering

May 2010
Purdue University
Indianapolis, Indiana

I dedicate this thesis to my parents, brother and sister-in-law. Without their support, patience, and most of all love, the completion of this work would not have been possible.

ACKNOWLEDGMENTS

I owe my deepest gratitude to my parents, Dr. Dhirajlal Radadiya and Prabha Radadiya. Their patience, support, and most of all love, has been the key to my successful educational career.

I am indebted to my brother, Dr. Adarsh Radadia, and my sister-in-law, Deepa Radadia for their guidance, love and support. Adarsh has been my inspirational role model throughout this academic journey and his assistance has been an invaluable contribution towards the completion of this work.

I am grateful to my advisor Dr. Maher E. Rizkalla for his guidance and supervision during the entire course of this research and thesis work. I would like to thank him for providing an unflinching support in various ways and constant encouragement in hardship.

I would like to thank Anna Shiver (Technician, Engineering Technology) and Jeff Sears (Lab Coordinator, Electrical and Computer Engineering) for providing assistance with some of the electrical components required for the experimental setup.

I would like to thank Valerie Lim Diemer (Graduate Program Coordinator) and Sherrie Tucker (Office Coordinator, Electrical and Computer Engineering) for their assistance in fulfilling the requirements towards the graduate degree.

I thank all my friends for their support and encouragement.

TABLE OF CONTENTS

Page

LIST OF TABLES

LIST OF FIGURES

Figure Page

ABSTRACT

Radadia, Jasmin Dhirajlal. M.S.E.C.E, Purdue University, May, 2010. A Highly Precise and Linear IC for Heat Pulse Based Thermal Bidirectional Mass Flow Sensor. Major Professor: Maher E. Rizkalla.

In this work we have designed and simulated a thermal bi-directional integrated circuit mass flow sensor. The approach used here was an extension to the gas flow model given by Mayer and Lechner [1]. The design features high precision response received from analog integrated circuits.

A computational fluid dynamic (CFD) model was designed for simulations with air and water Using COMSOL Multiphysics. Established mathematical models for the heat flow equations including CFD parameters were used within COMSOL simulation (COMSOL Multiphysics, Sweden). Heat pulses of 55 °C for a period of nearly 120 seconds and 50% duty cycles were applied as thermal sources to the flowstream. The boundary conditions of the heat equations at the solid (heating element) fluid interface were set up in the software for the thermal response.

The hardware design included one heating element and two sensing elements to detect the bi-directional mass flow. Platinum sensors were used due to their linear characteristics within 0 ºC to 100 ºC range, and their high temperature coefficient (0.00385 Ω/Ω/ºC). Polyimide thinfilm heater was used as the heating element due to its high throughput and good thermal efficiency. Two bridge circuits were used to sense the temperature distribution in the vicinity of the sensing elements. Three high precision instrumentation low power amplifiers with offset voltage ~2.5μV (50μV max) were used

for bridge signal amplification and the difference circuit. The difference circuit was used to indicate the flow direction. A LM555 timer chip was utilized to provide the heat pulse period.

Simulation and experimental measurements for heat pulses with different amplitude (temperature) were in good agreement. Also, the sensitivity of the flow sensor was observed to remain unaffected with the change in the duty cycle of the heat operation mode.

1. INTRODUCTION

1.1 Problem Statement

The evolution of thermal mass flow technology began sometime in late the 1950's. The development and commercialization of mass flow measuring meter based on the thermal flow measurement principle began and gained wide acceptance in the industrial sector. The thermal mass flow meters had the capability to measure low and varying mass flow rates directly, and their great accuracy in measuring the mass flow led to the replacement of other older technologies in the field [2]. With the development of the thermal flow meters, additional features such as ability to compute multi-point flow averaging, inline flow meters, built-in flow conditioning, and ultra-clean construction made them the preferable choice in industrial applications like air flow measurement, process industries with gas reactions, semiconductor industries, just to name a few.

Constant improvisation in the thermal mass flow technology has been observed in order to achieve highest accuracy, linearity and lowest power consumption possible. A conventional thermal mass flow sensor employs a constant power source to heat a heating element which is either exposed to the fluid flow, in case of invasive sensor design, or indirectly heats the fluid flow, in case of noninvasive design [3, 4, 5]. Therefore, to conserve energy, an alternative to the constant power source has to be designed and implemented such that the accuracy of the outcome and the reliability of the sensors are not affected.

In summary, the current flow devices lack low power consumption, flexibility (multifunctional for gases and liquids), and bi-directional flow rate detection.

1.2 Previous Work

The heat/thermal pulse technique is employed by majority of the thermal mass flow sensors operating based on the principle of thermal time of flight. Bauer (1965) was the first recorded to use the pulsed-wire technique for flow measurement. Bauer's method used two wire mounted perpendicular to each other and applied a square-wave pulse to one wire [6]. In his claim he was able to compute the average velocity based on the Equation 1.1:

$$\mathrm{U_m} = \frac{\Delta \mathrm{x}}{\Delta \mathrm{t_f}} \tag{1.1}$$

where:

U_m is the measure velocity of the fluid

Δx is the distance between the hot wires

$\Delta \mathrm{t_f}$ is the time of flight

Further work in the same direction was carried out by Tomback (1969), Bradbury and Castro (1971) [7]. These works were all in the attempt to increase the dynamic range of the thermal time of flight mass flow sensors. In 1982, Boyd [8] utilized a heat pulse technique in his invention of a mass flow meter. His invention was comprised of a temperature sensor, a reference resistor, a low and high voltage source, and a pulse controller. The latter is used for the circuit control and thereby provide signal to the temperature sensor and the reference resistor. The operation of this device was similar to a hot wire anemometer based on King's (1914) analysis which states that the rate of heat transfer is directly proportional to the Reynolds Number and can be described by the Equation 1.2:

$$H = A + BR_e^{\alpha} P_R^{\beta} \tag{1.2}$$

where:

H is the thermal transfer coefficient

A & B are constants

R_e^{α} is the Reynolds Number

α is the Reynolds power

P_R^{β} is the Prandtl Number

β is the Prandtl power

The Reynolds number can be expressed by the equation:

$$R_e = EW/d\mu \tag{1.3}$$

where:

E is a constant

W is the mass flow rate

D is the pipe inside diameter

μ is the fluid viscosity

Boyd applied both, a low voltage pulse and a high voltage pulse, to the temperature sensor. He measured the voltage drop across the temperature sensor and the reference resistor. From this data, the temperature of the respective temperature sensor and reference resistor is calculated, which is further used to calculate the thermal transfer coefficient as the input to the sensor is known. The Reynolds number can be calculated using the thermal transfer coefficient which can be further used to compute the mass flow rate of the fluid. The delay between the heat pulse and electrical response represents a drawback to this system. Other researchers have come up with similar approaches but their ideas lack optimum power consumptions.

With the advancement of new technology in hardware and software, an improvement in the sensor design helped reduce the complexities in the flow

measurement and calibration of circuits. Furthermore, new materials have showed a promising linearity needed for thermal sensors. The data acquisition technology has helped to interface sensors with the computer systems. In 1998, Mayer and Lechner [1] claimed an invention of low power consumption mass flow sensor. The device was fabricated on a single silicon crystal. An opening was etched and covered with a dielectric membrane. The assembly consisted of two thermopiles placed symmetrically, one on each side of a resistive heating element. The flow meter was operated in cycles, to reduce the power consumption. The pulsed mode was carried out in cycles by applying a current pulse till a certain time period that would allow the thermopile pair to reach equilibrium. Then no pulse was applied for a time period that was five times, preferably at least ten times, longer than the first pulse. The operation of this flow sensor was based on the Calorimetric flow measurement principle. The temperature difference signal of the two thermopiles was measured. Results were dependent on the flow velocity, density of the fluid, and pressure. The mass flow was further computed using the calibration tables.

1.3 Thesis Objectives

This thesis particularly focuses on mass flow measurement using the thermal flow technique in closed conduits. The objective of this research project is to contribute to the existing idea of power conservation in the thermal mass flow sensor operation. The earlier work of Mayer and Lechner [1] on gas flow measurement was extended to model fluid flow simulations. This objective has been accomplished by constructing a Computational Fluid Dynamic (CFD) model for gas (air) and liquid (water).

In order to verify the CFD model data, an experimental in-lab mass flow sensor was designed. Experimental data supporting the CFD model data for gas (air) was further obtained. An attempt to experiment the current apparatus for liquids is under progress.

2. FLOW MEASUREMENT TECHNOLOGY

This chapter presents various methodologies for the fluid flow measurement, utilizing different sensor technologies. This study assists with the selection leading to optimum power consumption, high precision, and bi-directional flow system.

Numerous industrial applications require a precisely controlled fluid flow. Depending on various flow conditions encountered in different applications, varieties of principles are applied to measure the flow rate of the fluids. Currently, various types of flow measurement sensors are available [9, 10, 11]. The flow sensors can structurally be distinguished as invasive and non-invasive types. Furthermore, based on their principle of operations some of the flow sensors can be classified as differential pressure, positive displacement, velocity, thermal, etc. Out of all these existing flow sensors only the ones that are commonly prevalent are discussed below.

Before understanding the principles of each flow sensor, it is necessary to understand the dynamic properties of fluid flow in closed conduits [12]. Fluid motion in a closed piping system can be characterized as one of the two main types: Laminar or Turbulent flow. In some cases combinations of both types of motions have been observed. In Laminar flow, the fluid travels in layers (in the axis parallel to the walls of the pipe), that do not mix as they move in the direction of the flow. The Laminar flow is also referred as streamline flow. In Turbulent flow, the fluid moves in a random course with only the average motion of the fluid being parallel to the axis of the pipe. Figure 2.1 shows the laminar and turbulent flows.

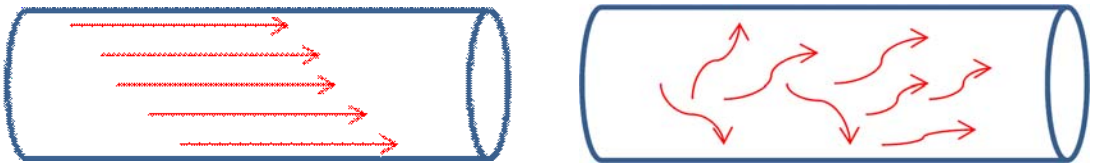

Figure 2.1 Closed conduit flow types

Our focus will be given to the Laminar flows where the Reynolds number is below 1000. The Reynolds number is a dimensionless number and can be used to predict the flow characteristics of a fluid. It is useful in characterizing the flow types. In Laminar flows the Reynolds number is lower as the viscous forces are dominant, while in Turbulent flows, the Reynolds number is higher as the inertia forces are dominant.

Reynolds number can be calculated as shown in Equation 2.1:

$$R_e = \frac{\rho \bar{v} D}{\eta} \tag{2.1}$$

where:

R_e is the Reynolds number

P is the density of the fluid

$\bar{v}$ is the mean velocity of the fluid

D is the pipe diameter

η is the dynamic viscosity of the fluids

2.1 Differential Pressure Flow Sensors

Differential pressure type flow sensors are the most commonly used instruments, especially for liquid flow measurements [13]. The operational principle of differential pressure flow sensors is based on the Bernoulli's equation of fluid dynamics [12]. When

fluid is passed through a pipe with different cross sectional area, a change in the pressure and velocity profile of the fluid takes place following Bernoulli's equation.

Figure 2.2 shows the basis of Bernoulli's equation.

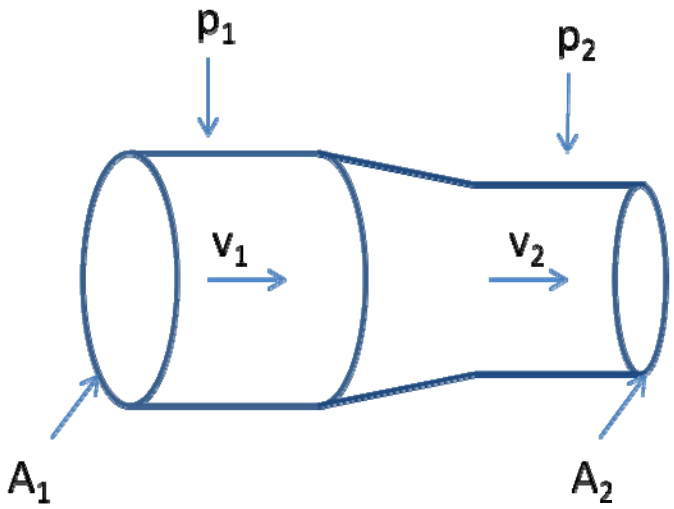

Figure 2.2 Conduit schematics to exemplify Bernoulli's principle

In case of horizontal pipes, Bernoulli's equation reduces to Equation 2.2:

$$\frac{p_1 - p_2}{\rho} = \frac{v_1^2 - v_2^2}{2} \tag{2.2}$$

where:

p_1 is the pressure before the restriction

p_2 is the pressure after the restriction

v_1 is the velocity before the restriction

v_2 is the velocity after the restriction

ρ is the fluid density

The volumetric flow rate (Q) of the fluid can be determined by using the Conservation of mass principle given by Equation 2.3:

$$v_1 A_1 \rho = v_2 A_2 \rho \tag{2.3}$$

where:

A_1 is the cross sectional area of the pipe before restriction

A_2 is the cross sectional area of the pipe after restriction

Therefore,

$$Q = v_1 A_1 = \frac{A_2}{\sqrt{1 - (\frac{A_2}{A_1})^2}} \sqrt{\frac{2(p_1 - p_2)}{\rho}} \tag{2.4}$$

The most commonly used flow sensors based on the differential pressure principle in industry are orifice plate, flow nozzles, venture tubes and variable area-rotameters [14]. Some drawbacks were cited with these flow measurement sensors. The drawbacks include cost effectiveness issue, sensitivity, accuracy, bulk use devices.

2.2 Positive Displacement Flow Sensors

The fluid flow component under measure, in Positive Displacement (PD) type flow sensors, is the volume rate of the fluid that flows through the pipe [12]. This type of flow sensors employs a mechanism with a chamber like structure. In this scheme, a known volume of fluid is entrapped and releases back into the flow stream. The volume flow rate of the flow stream can be computed by taking measurement of the total number of entrapments over a unit period of time. The PD flow sensors are used for gas and liquid flow measurement. More interestingly a PD flow sensor can be used to measure low gas or liquid flows without any external power being supplied. Despite the internal

moving mechanical components being mass-calibrated, the positive displacement flow sensor tends to be hydraulically imbalanced [15]. The PD sensor absorbs a small amount of energy from the flow stream and thereby drives its internal assembly.

Some of the commonly used PD flow sensors in industry are oscillating piston, nutating disc, oval gear, vane, rotor, roots and multi-piston. Furthermore, these kinds of sensors are not favorable for use due to their non-invasive structure with additional mechanical components needed to perform the measurements.

2.3 Velocity Flow Sensor

In the velocity flow sensors, the velocity parameter of the fluid flow is the basis of the measurement. This is due to the fact that fluid velocity is directly proportional to the volume flow rate [12]. These types of flow sensors use transducers that convert any physical changes in the system into electrical signals. The electrical parameters, such as power, frequency and phase, change with the physical changes of the system. These parameters can be analyzed and used to compute the velocity of the flowstream. Some of the most commonly used velocity flow sensors are turbine, vortex shedding, swirl, electromagnetic, ultrasonic (Doppler and transit-time), etc. The non linearity between flow, pressure, and velocity may cite some errors in measurements utilizing these sensors.

2.4 Mass Flow Sensors

The mass flow sensors are measuring units that directly measure the mass flow rate of the fluid flow through a unit cross section. The working range of this type of sensor depends on the fluid properties such as specific heat, density and temperature but is independent of the physical state of the fluid.

2.4.1 Coriolis Flow Sensors

These types of flow sensors give a direct mass flow measurement based on the change in the vibration of the tube through which the fluid under measurement is passed. The drawbacks of such sensors include larger size, high maintenance, and high installation costs [16].

2.4.2 Thermal Mass Flow Sensor (TMFS)

Thermal flow sensors are basically transducers, that comprise of both heaters and temperature sensors that are placed in a manner such that the streaming fluid carries some heat in the direction of the flow. This causes the temperature distribution to change around the temperature sensor. This is attributed to the heat transfer in the vicinity of the sensor. The evaluation of the heat transfer is conducted in different ways depending on the operating modes of a thermal flow sensor. Fluids with constant density and specific heat properties can be measured without sensor calibrations. On the other hand, fluids with varying density and specific heat properties have to be calibrated for additional pressure temperature compensation. There are three basic categories for the thermal mass flow sensors: anemometric, calorimetric, and thermal time of flight sensors [17].

2.4.2.1 Anemometric Flow Sensors

Generally, anemometer consists of single element, which is submerged in the streaming fluid and heated by an electrical signal. The element temperature is maintained above the ambient temperature. With any flow, the heat dissipated by the element will be carried over in the direction of the flow. The influence of the flow on the element temperature is measured by measuring the resistivity of the element. Hot wire or hot film anemometers have very fast response times due to their appropriate thermal mass. Figure 2.3 show the common arrangement of anemometric flow sensor.

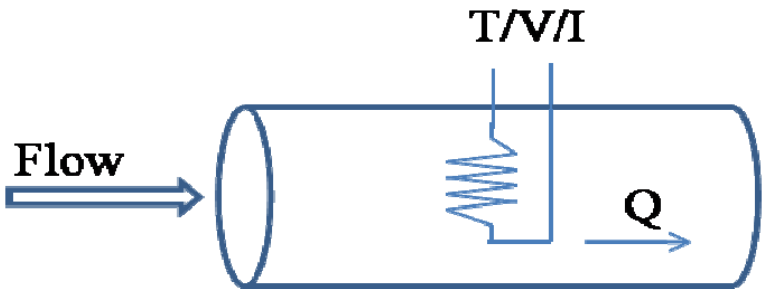

Figure 2.3 Schematic of one element arrangement Anemometer

Anemometers can be operated in the following modes [18]:

Constant power mode: In this mode, a constant power is supplied to heat a resistive element which further dissipates heat into the streaming fluid. The resulting temperature of the resistor is used as a measure to calculate the fluid flow rate. Higher the flow, lower is the temperature of the resistive element.

Constant temperature mode: In this mode, the temperature of the heating element is measured and maintained constant above the ambient temperature. The electrical power required to maintain the heating element at a constant temperature is used as a measure to calculate the fluid flow rate.

Temperature balance mode: In this mode, two resistive elements are used, up- and downstream. The temperature difference between the two heating elements is kept constant by controlled distribution of a constant total heating power. The ratio of the up- and downstream heating power is used as a measure to calculate the fluid flow rate. The advantage of this mode is that the system output is independent of the sensitivity of the sensors. Figure 2.4 shows the temperature balance mode of the anemometer sensor with differential temperature displayed.

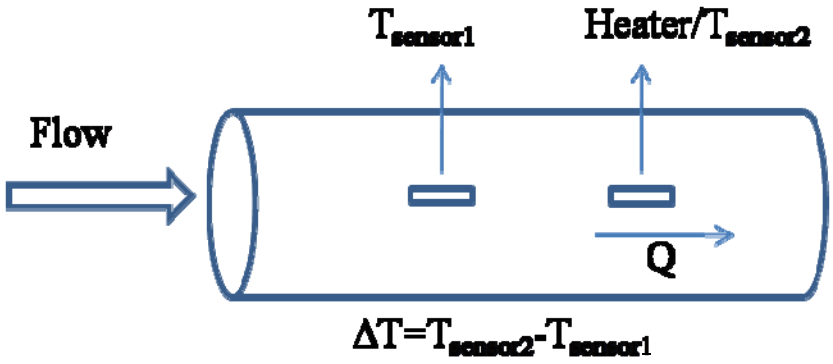

Figure 2.4 Schematic layout of anemometer sensor in balance mode

2.4.2.2 Calorimetric Flow Sensors

Calorimetric flow sensors require a minimum of two or more elements. A standard arrangement, as shown in Figure 2.5, consists of a heating element aligned symmetrically between two sensing elements, up- and downstream, hence permits the sensors to be used for bidirectional fluid measurements. The differential temperature measurement of the two sensing elements, up- and downstream, is used as a measure to calculate the fluid mass flow rate. When there is no flow present, the temperature profile is symmetrical around the heater. These types of flow sensors have higher application in measuring low flow rates. Equation 2.5 gives the mass flow rate:

$$\dot{m} = \frac{\dot{H}}{C_p \Delta T} \tag{2.5}$$

where:

$\dot{m}$ is the mass flow rate of the gas

$\dot{H}$ rate of heat transfer

C_p is the specific heat of the fluid under constant pressure

ΔT is the temperature difference across the heated section

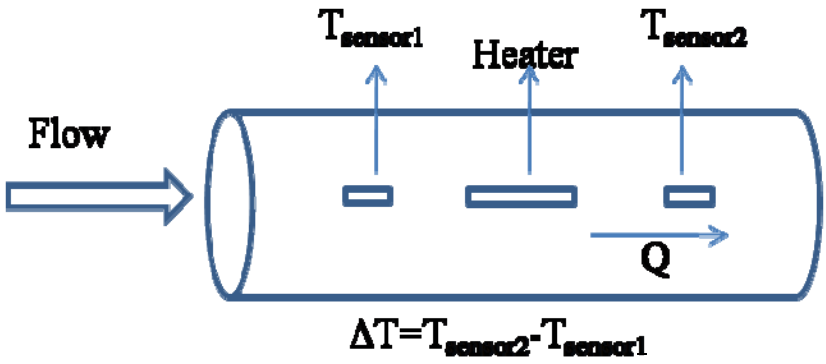

Figure 2.5 Schematic layout of a calorimetric sensor

2.4.2.3 Thermal Time of Flight Sensor (TTOF)

TTOF sensors require a minimum of two elements. The configuration of the TTOF sensor elements is quite similar to that of the Calorimetric flow sensor. In this type of sensors, the heater is applied a constant pulse of an electrical energy. The heat pulse dissipated from the heater is carried away by the streaming fluid in the direction of the flow where the temperature sensor is placed to measure heat pulse. The time interval between the application of the electrical pulse and arrival of the heat pulse at the temperature sensor is called the Time of Flight. Since the distance between the heater and the temperature sensor is fixed, the Time of Flight provides the measure to calculate the fluid flow rate. The velocity can be computed based on Equation 2.6:

$$U = \frac{x}{\Delta t} \tag{2.6}$$

where:

U is the velocity of the fluid

x is the distance between the heater and the sensor

Δt is the time of flight of the pulse from the heater to the sensor

Figure 2.6 gives the common arrangement of TTOF sensors.

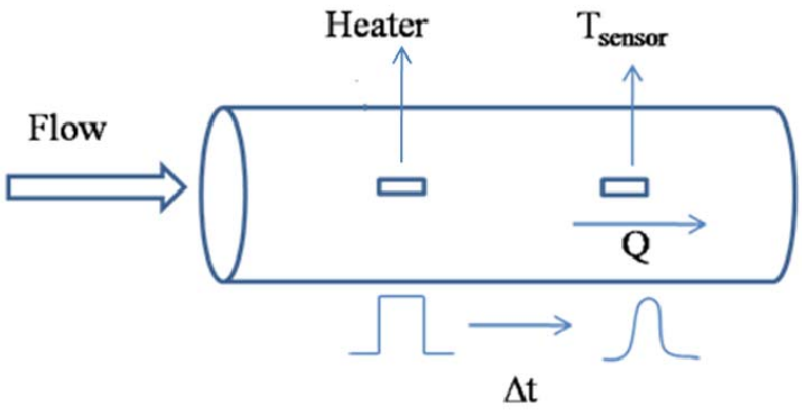

Figure 2.6 Schematic layout of a thermal time-of-flight sensor

2.4.2.4 Conclusion

The conventional TMFS (anemometer) have been observed to use continuous power in all operational modes. Continuous power requirement reduces the flexibility of the flow sensor. TTOF sensors consume less power comparatively. But both types of TMFS are restricted to unidirectional flow sensing. Calorimetric TMFS can be used to for bi-directional flow sensing.

3. MATHEMATICAL MODELS OF HEAT AND MASS TRANSFER

In this chapter the solutions of heat equations as applied to conduction and convection heat transfer are described. The results of these solutions lead to the temperature distribution within the fluid. Because of the small size of the sensing elements (thinfilm Platinum RTDs) and its good thermal conductivity, the conduction heat transfer is negligibly small. The convection heat transfer will be the major contributor to the temperature distribution within the flow around the sensors. The mathematical model covers a bidirectional heat transfer from the heating element to the sensors. These models have led to the boundary and subdomain settings for the CFD model simulated with COMSOL.

3.1 Conduction Heat Transfer

Conduction occurs due to presence of the temperature gradient within a medium. As a result, heat transfer within a medium takes place from a high temperature region to a low temperature region. This rate of heat flow (Q) is directly proportional to rate of change of temperature with respect to the distance and in the direction of the flow. The mathematical representation of the rate of heat flow is known as the Fourier's Law. The rate equation in one-dimensional plane can be expressed by Equation 3.1:

$$\frac{dQ}{dt} = -\rho A \frac{\partial T}{\partial x} \tag{3.1}$$

where:

ρ is the thermal conductivity of the medium

A is the area normal to the direction of the flow

T is the temperature of the medium

The negative sign in the above equation is due to the direction of the heat transfer towards the decreasing temperature. For steady state heat conduction, the heat transfer per unit area, also known as the heat flux ($\ddot{q}$) can be given by Equation 3.2 [19]:

$$\ddot{q} = -\rho \frac{\partial T}{\partial x} \left(\frac{W}{m^2}\right) \tag{3.2}$$

For homogeneous and isotropic materials the general unsteady state heat conduction equation in a three dimensional plane can be expressed in the Cartesian coordinates as:

$$\frac{\partial^2 T}{\partial x^2} + \frac{\partial^2 T}{\partial y^2} + \frac{\partial^2 T}{\partial z^2} + \frac{q_g}{k} = \frac{1}{\alpha}\frac{\partial T}{\partial t} \tag{3.3}$$

where:

q_g is the heat generation rate per unit volume

k is the thermal conductivity of the material

α is the thermal diffusivity

Now if the flow is in steady state (*i.e.*$\frac{\partial T}{\partial t} = 0$) and if there is no internal heat generation in the material (*i.e.*$q_g = 0$), then the governing equation can be expressed as:

$$\frac{\partial^2 T}{\partial x^2} + \frac{\partial^2 T}{\partial y^2} + \frac{\partial^2 T}{\partial z^2} = 0 \tag{3.4}$$

3.2 Convection Heat Transfer

In presence of a temperature gradient in a liquid medium, convection occurs, causing actual movement of fluid molecules from a high temperature region to a low temperature region (diffusion). Also, in convection, the transfer of energy takes place due to bulk/macroscopic motion of fluids [19]. There are two types of convections: natural convection and forced convection. In natural convection the flow is caused due to buoyancy effects in the fluid while in case of forced convection an external source (fan, pump, etc.) causes the flow.

Irrespective of the nature of convection the heat flow rate equation can be expressed using the Newton's law of cooling as shown in Equation 3.5:

$$q = hA(T_s - T_\infty) \tag{3.5}$$

where:

q is the rate of heat transfer by convection (W)

h is the average convective heat transfer coefficient (W/m^2K)

A is the heat transfer surface area (m^2)

T_s is the temperature of the solid surface (°C)

T_∞ is the temperature of the fluid free stream (°C)

The heat flux rate ($\ddot{q}$) can be expressed as show in Equation 3.6:

$$\ddot{q} = h(T_s - T_\infty) \quad (\frac{W}{m^2}) \tag{3.6}$$

General statements of the conservation of energy laws play an important role in the analysis of heat transfer due to convection. One dimensional flow rate equation is given as in Equation 3.7:

$$m = \rho AV \tag{3.7}$$

where:

m is the mass flow rate of fluid

ρ is the fluid density

V is the normal velocity

A is the flow area

The law of conservation of mass as applied to an element in Cartesian coordinates can be expressed as [20]:

$$\frac{\partial \rho}{\partial t} + \frac{\partial}{\partial x}(\rho u) + \frac{\partial}{\partial y}(\rho v) + \frac{\partial}{\partial z}(\rho w) = 0 \tag{3.8}$$

where:

u, v and w are the velocity components in the x, y and z-direction

This is called the continuity equation. An alternative form of this equation is given as in Equation 3.9:

$$\frac{\partial \rho}{\partial t} + \nabla \cdot \partial \vec{V} = 0 \tag{3.9}$$

where:

$\vec{V}$ is the velocity vector

The law of Conservation of momentum: The Navier-Strokes equations of motion for Newtonian fluids are given as in Equations 3.10, 3.11, and 3.12:

$$\rho \frac{Du}{Dt} = \rho g_x - \frac{\partial p}{\partial x} + \frac{\partial}{\partial x}\left[\mu\left(2\frac{\partial u}{\partial x} - \frac{2}{3}\nabla \cdot \vec{V}\right)\right] + \frac{\partial}{\partial y}\left[\mu\left(\frac{\partial u}{\partial y} + \frac{\partial v}{\partial x}\right)\right] + \frac{\partial}{\partial z}\left[\mu\left(\frac{\partial w}{\partial x} + \frac{\partial u}{\partial z}\right)\right] \tag{3.10}$$

$$\rho\frac{Dv}{Dt}=\rho g_y-\frac{\partial p}{\partial y}+\frac{\partial}{\partial y}\left[\mu\left(2\frac{\partial v}{\partial y}-\frac{2}{3}\nabla\cdot\vec{V}\right)\right]+\frac{\partial}{\partial z}\left[\mu\left(\frac{\partial v}{\partial z}+\frac{\partial w}{\partial y}\right)\right]+\frac{\partial}{\partial x}\left[\mu\left(\frac{\partial u}{\partial y}+\frac{\partial v}{\partial x}\right)\right] \tag{3.11}$$

$$\rho\frac{Dw}{Dt}=\rho g_z-\frac{\partial p}{\partial z}+\frac{\partial}{\partial z}\left[\mu\left(2\frac{\partial w}{\partial z}-\frac{2}{3}\nabla\cdot\vec{V}\right)\right]+\frac{\partial}{\partial x}\left[\mu\left(\frac{\partial w}{\partial x}+\frac{\partial u}{\partial z}\right)\right]+\frac{\partial}{\partial y}\left[\mu\left(\frac{\partial v}{\partial z}+\frac{\partial w}{\partial y}\right)\right] \tag{3.12}$$

The above three equations can be combined to be expressed in the vector form as in Equation 3.13:

$$\rho\frac{D\vec{V}}{Dt}=\rho\vec{g}-\nabla\vec{p}+\frac{4}{3}\nabla\left(\mu\nabla\cdot\vec{V}\right)+\nabla\left(\vec{V}\cdot\nabla\mu\right)-\vec{V}\nabla^2\mu+\nabla\mu\times\left(\nabla\times\vec{V}\right)$$
$$-\left(\nabla\cdot\vec{V}\right)\nabla\mu-\nabla\times\left(\nabla\times\mu\vec{V}\right) \tag{3.13}$$

This equation is simplified when applied to following cases:

Case 1: Constant viscosity as given in Equation 3.14.

$$\rho\frac{D\vec{V}}{Dt}=\rho\vec{g}-\nabla\vec{p}+\frac{1}{3}\mu\nabla\left(\nabla\cdot\vec{V}\right)+\mu\nabla^2\vec{V} \tag{3.14}$$

Case 2: Constant viscosity and density as given in Equation 3.15.

$$\rho\frac{D\vec{V}}{Dt}=\rho\vec{g}-\nabla\vec{p}+\mu\nabla^2\vec{V} \tag{3.15}$$

where:

μ is a property called viscosity and

p is the hydrostatic pressure

The law of conservation of energy or the energy equation for heat transfer is given as in Equation 3.16:

$$\rho c_p \frac{DT}{Dt} = \nabla \cdot k\nabla T + \beta T \frac{Dp}{Dt} + \mu\emptyset \tag{3.16}$$

where:

c_p is the specific heat of constant pressure

k is the thermal conductivity

p is the pressure

β is the coefficient of thermal expansion and is defined as in Equation 3.17:

$$\beta = -\frac{1}{\rho}\left[\frac{\partial \rho}{\partial T}\right]_p \tag{3.17}$$

$\emptyset$ is the energy dissipation function due to friction and in Cartesian coordinates can be given as in Equation 3.18:

$$\emptyset = 2\left[\left(\frac{\partial u}{\partial x}\right)^2 + \left(\frac{\partial v}{\partial y}\right)^2 + \left(\frac{\partial w}{\partial z}\right)^2\right] + \left[\left(\frac{\partial u}{\partial y} + \frac{\partial v}{\partial x}\right)^2 + \left(\frac{\partial v}{\partial z} + \frac{\partial w}{\partial y}\right)^2 + \left(\frac{\partial w}{\partial x} + \frac{\partial u}{\partial z}\right)^2\right]$$

$$-\frac{2}{3}\left(\frac{\partial u}{\partial x} + \frac{\partial v}{\partial y} + \frac{\partial w}{\partial z}\right)^2 \tag{3.18}$$

The above equations can be further simplified for the following cases:

Case 1: Incompressible fluids as given in Equation 3.19.

$$\rho c_p \frac{DT}{Dt} = \nabla \cdot k\nabla T + \mu\emptyset \tag{3.19}$$

Case 2: Incompressible constant conductivity fluid as given in Equation 3.20.

$$\rho c_p \frac{DT}{Dt} = k\nabla^2 T + \mu\emptyset \tag{3.20}$$

Case 3: Ideal gas law as given in Equation 3.21.

$$\rho c_v \frac{DT}{Dt} = \nabla \cdot k\nabla T - p\nabla . \vec{V} + \mu\emptyset \tag{3.21}$$

where:

c_v is the specific heat at constant volume

3.3 Radiation Heat Transfer

In some cases the heat transfer takes place through radiations or waves without any need of an intermediate medium present between the two elements. However, the radiation heat transfer is not important in case of thermal calorimetric flow sensors due to the relatively low magnitude of the thermal wavelengths [12].

3.4 Analytical Model for Intrusive Type Design Calorimetric Mass Flow Sensor

In an invasive type design calorimetric mass flow sensor the heating element and a pair of sensing elements come in direct contact with the flow stream of the fluid to be measured. Hence the heat transfer in this kind of a setup would take place either by conduction through fluid particles, or by convection through the fluid thermal mass. The temperature distribution can be determined by the applying the energy conservation requirements [12].

Consider a homogeneous medium whose temperature distribution T(x,y,z) can be expressed in the Cartesian coordinates. The heat diffusion equation in the Cartesian coordinates for such a homogeneous medium can be expressed as Equation 3.22:

$$\frac{\partial^2 T}{\partial x^2} + \frac{\partial^2 T}{\partial y^2} + \frac{\partial^2 T}{\partial z^2} + \frac{\dot{q}}{k} = \frac{1}{\alpha}\frac{\partial T}{\partial t} \tag{3.22}$$

where:

$\dot{q}$ is the rate at which energy is generated per unit volume of the medium. (W^3/m)

k is the thermal conductivity of the medium. (W/K*m)

$\alpha = \frac{k}{\rho c_p}$ is the thermal diffusivity of the fluid

ρ is the density of the fluid

c_p is the specific heat of the fluid

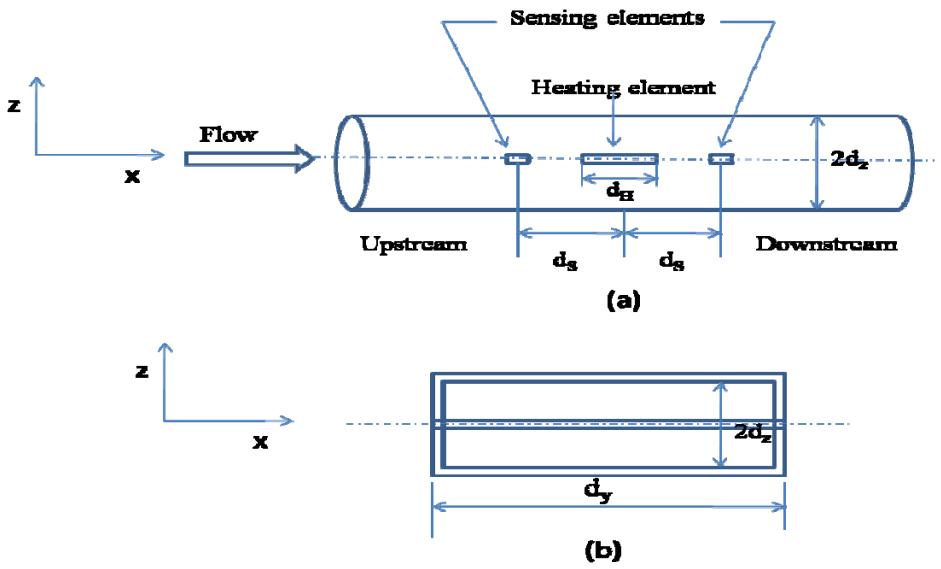

Figure 3.1 (a) Horizontal section, and (b) Cross-section

An analytical model for calorimetric sensor is described by Nam-Trung Nguyen [12]. The temperature profile in the *y* and *z* directions is assumed to be constant and linear, hence simplifying the analysis to one dimension. Refer Figure 3.1, consider the cross section of the sensor whose area (A) can be given as $d_y 2d_z$. Let the average fluid velocity be given as '*v*'. Hence the heat diffusion equation can be reduced and rewritten as Equation 3.23:

$$\frac{\partial^2 T}{\partial^2 x} - \left(\frac{v}{\alpha}\right)\frac{\partial T}{\partial x} - \frac{T}{d_z^2} = 0$$

(3.23)

The above equation is linear in temperature and can be solved with the boundary condition as given in Equation 3.24:

$$\log_{x \to \pm\infty} T(x) = 0$$

(3.24)

The obtained temperature distribution results are shown in Equations 3.25 - 3.29:

$$T(x) = T_0 e^{\left[\gamma_1\left\{x + \frac{d_H}{2}\right\}\right]} \; for \; x < \frac{-d_H}{2}$$

(3.25)

$$T(x) = T_0 e^{\left[\gamma_2\left\{x - \frac{d_H}{2}\right\}\right]} \; for \; x > \frac{d_H}{2}$$

(3.26)

$$\frac{d_H}{2} < x < \frac{-d_H}{2} \; for \; T(x) = T_0$$

(3.27)

where,

$$\gamma_{1,2} = \frac{\left(v \pm \sqrt{v^2 + \frac{2a^2}{d_z^2}}\right)}{(2a)}$$

(3.28)

$$T_0 = \frac{Q}{\left[\left(\frac{2\lambda d_y d_H}{d_z}\right) + A\lambda(\gamma_1 - \gamma_2)\right]}$$

(3.29)

The temperature difference between the upstream sensor and the downstream sensor can be computed as shown in Equation 3.30:

$$\Delta T(v) = T_0 \left\{ e^{\left[\gamma_2\left(\frac{d_s - d_H}{2}\right)\right]} - e^{\left[\gamma_1\left(\frac{-d_s + d_H}{2}\right)\right]} \right\} \tag{3.30}$$

3.5 Finite Element Analysis

COMSOL uses the Finite Element Method (FEM) for discretization of any given problem and further simplifies the problem to make it suitable for numerical computation (COMSOL Multiphysics, Sweden). The FEM analysis can be understood step by step as:

Step 1: Setting the Mesh

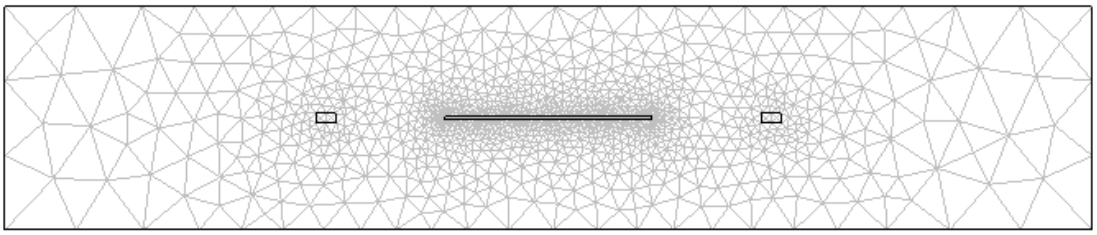

Figure 3.2 Triangular mesh elements in sensor geometry

First, a given element geometry is partitioned into small units of simple shape. This structure of small partitions is referred as mesh. In case of two dimensional analyses the element geometry is partitioned approximately into small triangular shape mesh elements as shown in Figure 3.2. The sides and corners of these triangles are known as mesh edges and mesh vertices. The mesh vertices are also known as node points.

Step 2: The Finite Elements

Once the meshing is complete, approximation of dependent variables is done by describing a function with a finite number of parameters in order to generate a system of equations for the Degree of Freedom (DOF).

An example:

For simplicity, consider a single variable '*u*' in 1 dimensional finite element space corresponding to quadratic elements. Assume a mesh with node points $x_1 = 0$, $x_2 = 1$, $x_3 = 2$, $x_4 = 0.5$ and $x_5 = 1.5$. The continuous function u is linear and a second order polynomial on each interval of the mesh. The corresponding DOF of u can be given as $U_i = u(x_i)$.

Hence, the 2nd order polynomial function u(x) on the mesh midpoints and endpoints is given as Equation 3.31:

$$u(x) = U_1\varphi_1(x) + U_2\varphi_2(x) + U_3\varphi_3(x) + U_4\varphi_4(x) + U_5\varphi_5(x) \tag{3.31}$$

where:

$\varphi_1(x)$ is called the Basis function which equals 1 at all i[th] node points and equals 0 at all other node points. For example in Equation 3.32:

$$\varphi_1(x) = \begin{cases} (1-x)(1-2x) & for\ 0 \le x \le 1 \\ 0 & for\ 1 \le x \le 2 \end{cases} \tag{3.32}$$

The Basis functions can further be expressed in simpler form using the element coordinates and the standard d-directional simplex $(\xi_1 \ge 0, \xi_2 \ge 0 \ldots \xi_d \ge 0, \xi_1 + \ldots + \xi_d \le 1)$ of the mesh elements. Thus in the above example with quadratic elements in 1D, the basis function can be given as Equation 3.33:

$$\varphi = (1 - \xi_1)(1 - 2\xi_1), \qquad \varphi = 4\xi_1(1 - 2\xi_1), \qquad \varphi = \xi_1(2\xi_1 - 1) \tag{3.33}$$

Step 3: The Lagrange Element

Lagrange interpolation is used to approximate the PDE solutions of the problem. Consider a polynomial functions u, in a finite element space, of the degree k (k is a positive integer). Thus each mesh element u is a polynomial is of k^{th} order. Such functions are described using Lagrange points, of order k, with element coordinates as integer multiples of k^{-1}. For example in a triangular mesh, if the p_i is the number of node points, then the degree of freedom is given as $U_i = u(p_i)$ and a continuous basis function as $\varphi_i(x)$. Thus, you have Equation 3.34:

$$u = \sum_i U_i \varphi_i \tag{3.34}$$

The order k of the polynomial can be arbitrary, but the available numerical integration formulas usually limit the computation to $k \leq 5$. The Lagrange element of order 1 is called the linear element, and element of order 2 is called the quadratic element.

4. HARDWARE DESIGN

In this chapter the hardware design including electrical circuit components, material used for sensors and analog chips are covered. This included interface circuitries required to measure the change in the electrical property of sensor as a result of flowstream.

4.1 The Heating Element

A MINCO Polyimide Thermofoil flexible heater/Kapton heater was used as the heating element in this project. The heater is thin, lightweight and is suitable for the design purpose. The advantage of this heater is its increased throughput as the heater provides fast and efficient thermal response. Figure 4.1 shows the thinfilm polyimide/Kapton heater.

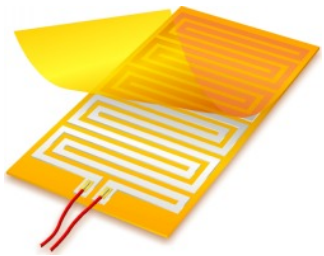

Figure 4.1 MINCO Polyimide Thermofoil heater/Kapton heater

The lead gauge of the heater is of size 30 as per the standardized American Wire Gauge (AWG) measurement. The heater has an Acrylic PSA backing. The operating range of the heater is from -30 °C to 100 °C with a maximum allowable watt density of

13 W (20 W/in^2). The effective area of the heater is 0.65 inch square. The resistance is about 6.2 Ohms with a tolerance of ±10% and a maximum allowable current of 3 A. The heater is operated on a DC supply of 2.5 V in pulse mode, with actual current of 0.403 A, and power output of 1 W.

Note: The selection of this heating element was based on the energy in Joule required to generate an appropriate temperature range between 35 °C to 80 °C sensed by the sensor. It shows linearity within various cycles.

4.2 The Temperature Controller

A miniature temperature controller (MINCO CT325) is used to control temperature of the heating element. The body of controller is filled with epoxy for moisture resistance. This controller offer simple control for flexible heating without needing any complex programming can help reduce the set-up time. The selection of this controller was based on its high precision in addition to its rated temperature (200 °C), covering the temperature range required for this project. The controller requires a RTD sensor to be attached to the heating surface of the heating element. The controller has a feedback system that takes an input from the RTD in order to control the heater output power. The Figure 4.2 shows the setup of the CT325 temperature controller. Terminals 1 and 2 are for the DC input power supply; terminals 5, 6 and 7 for RTD sensor input, and terminals 3 and 4 are for the heater output. The input power range of the controller is from 4.75 V to 60 V of DC supply with a maximum allowable current of 4 A.

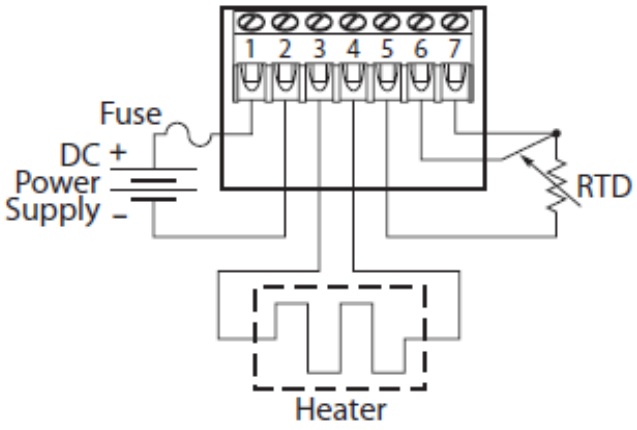

Figure 4.2 Schematic layout of the temperature controller setup

The setpoint temperature can be adjusted and read at $V_{setpoint}$ terminal and the actual heater output temperature can be monitored at the V_{temp} terminal using a voltmeter. The setpoint range of the controller is from 2 °C to 200 °C, and setpoint stability is ±0.02% of span/°C. The $V_{setpoint}$ and V_{temp} signal outputs corresponds to 0.010 V/°C over a specified range. Figure 4.3 shows the control pins for the CT325 temperature controller.

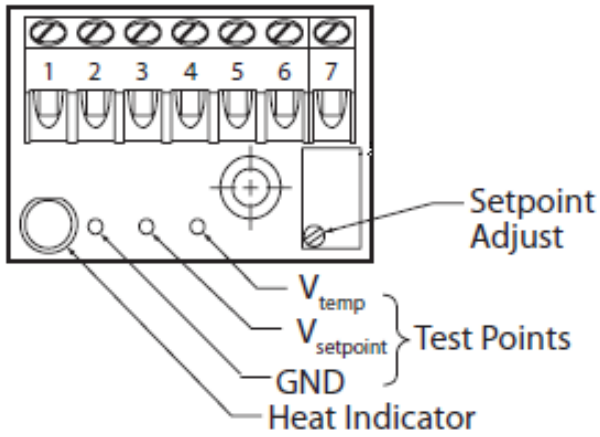

Figure 4.3 CT325 pins to control the temperature of the heating element connected

4.3 The Temperature Sensor

A pair of OMEGAFILM Platinum RTD elements (F3141) of class A is used as temperature sensing elements. RTD elements were chosen over thermocouple due to their ability to provide high accuracy. These thinfilm RTDs are made of IEC/DIN grade Platinum. Platinum metal shows great stability, repeatability and linearity in its resistance versus temperature characteristics. These thinfilm elements are of very small size and flat in shape. The temperature coefficient of resistance between 0 °C and 100 °C is 0.00385 Ω/Ω/°C. The RTD elements have temperature range from -70 °C to 600 °C and have a rapid response time**.** The resistance of the RTD elements is 1000.00 ±0.60 Ω at 0 ºC. Figure 4.4 shows the dimension of the thinfilm RTD.

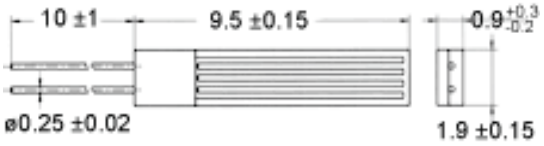

Figure 4.4 Schematic layout of the thinfilm Platinum RTD

An accurate model of resistance versus temperature function of the Platinum RTD elements can be give by using the Callendar-Van Dusen Equation [4.1]:

$$R_T = R_0 + R_0\alpha\left[T - \delta\left(\frac{T}{100} - 1\right)\left(\frac{T}{100}\right) - \beta\left(\frac{T}{100} - 1\right)\left(\frac{T}{100}\right)^3\right] \tag{4.1}$$

where:

R_T = Resistance at Temperature T

R_o = Resistance at T = 0ºC

α = Temperature coefficient at T = 0ºC ((typically +0.00392Ω/Ω/ºC))

δ = 1.49 (typical value for .00392 platinum)

β = 0 T > 0

0. 11 (typical) T < 0

According to DIN EN 60751 standards for class A type thinfilm RTDs the Callendar-Van Dusen equation can be reduced to Equation 4.2 and Equation 4.3:

$$For\ T \geq 0℃ \quad R(T) = R_0[1 + A.T + B.T^2] \tag{4.2}$$

$$For\ T < 0℃ \quad R(T) = R_0[1 + A.T + B.T^2 + C.(T - 100℃).T^3] \tag{4.3}$$

where:

A, B and C are Callendar-Van Dusen constants

$A = 3.9083 \cdot 10^{-3}\ °C^{-1}$

$B = -5.775 \cdot 10^{-7}\ °C^{-2}$

$C = -4.183 \cdot 10^{-12}\ °C^{-4}$

$R_0 = 1000\Omega$ measured at 0 °C

R(T) is the resistance at temperature T (°C)

4.4 Electrical Bridge Circuit

In general practice, to detect the change in the resistance with change in temperature, the RTDs are used in a simple Wheatstone bridge circuit as show in the Figure 4.5:

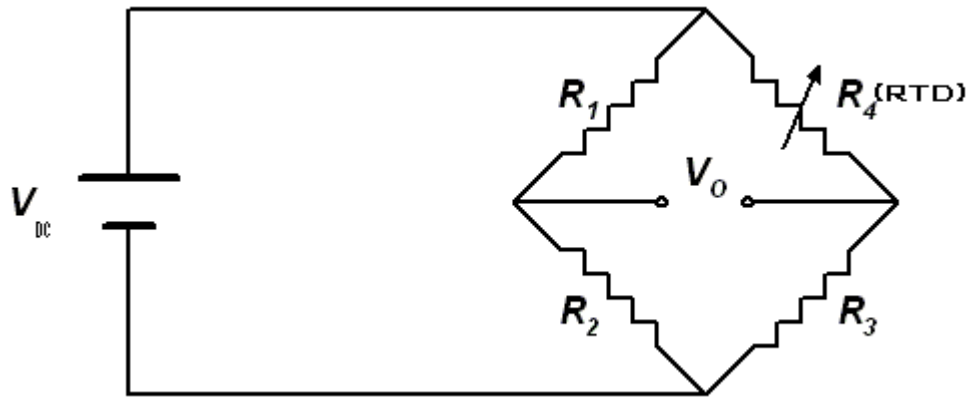

Figure 4.5 Simple Wheatstone bridge circuit with the sensing element

The Wheatstone bridge is excited by a 5 V DC supply. The bridge circuit is said to be balanced when the V_o signal gives a value zero. In order to balance the bridge circuit the resistor values are chosen such a way that the ratio of resistors R_2 over R_1 is equal to the ratio of resistors R_3 over $R_{4(RTD)}$ as shown in Equation 4.4:

$$\frac{R_2}{R_1} = \frac{R_3}{R_{4(RTD)}} \tag{4.4}$$

The resistance of the RTD elements at room temperature was measured to be about 1100 Ω hence the resistance values of R1, R2 and R3 were chosen as 1100 Ω in order have a balanced bridge circuit. The measured V_0 signal in the bridge circuit can be give in terms of input DC signal and the four resistors using the voltage divider rule as shown in Equation 4.5:

$$V_O = V_{DC}\left[\frac{R_{4(RTD)}}{R_3 + R_{4(RTD)}} - \frac{R_1}{R_1 + R_2}\right] \tag{4.5}$$

The resistance of the RTD sensor changes along with the temperature change. This change in the resistance can be calculated by solving Equation 4.5 for the RTD sensor. Equation 4.6 gives the change in sensor resistance.

$$R_{4(RTD)} = \frac{R_1 R_3 (V_{DC} + V_0) + R_2 R_3 V_O}{V_{DC}(R_1 + R_2) - V_O(R_1 + R_2) - V_{DC} R_1} \tag{4.6}$$

4.5 Instrumentation Amplifier

A low power, highly precise, instrumentation amplifier (INA128p) from Texas Instruments is used as a bridge signal amplifier and as a differential amplifier. The INA128 is a small size, laser trimmed, 8-pin plastic DIP with an inbuilt 3-op amp design that has a wide range of application. Figure 4.6 shows the pin configuration for INA128P. Figure 4.7 shows the 3-op amp design of INA128P.

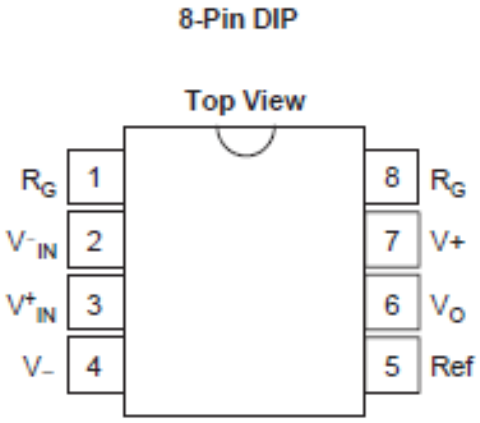

Figure 4.6 Pin configuration of the INA128p instrumentation amplifier

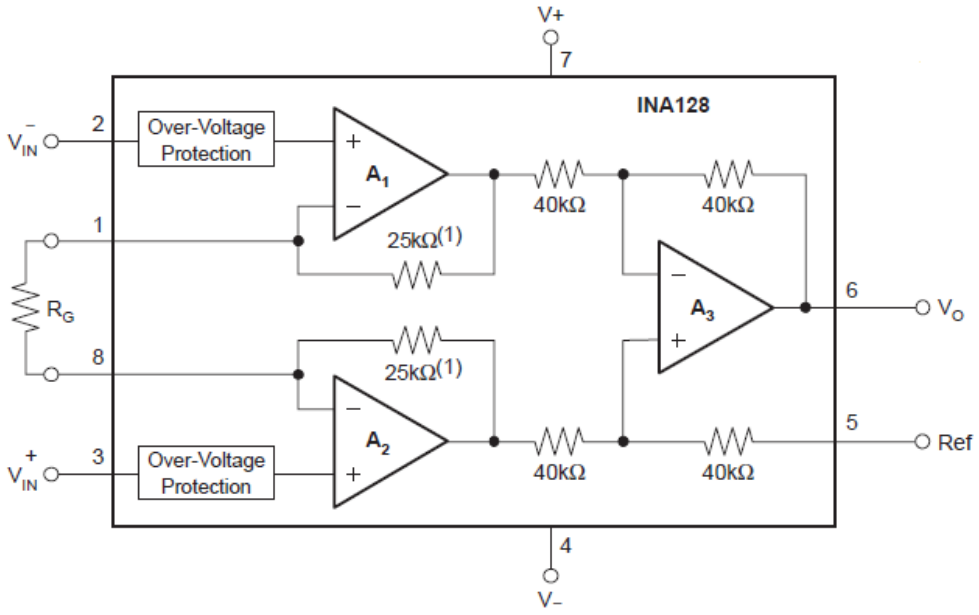

Figure 4.7 Schematic layout of the internal 3-op amp design of INA128p

The INA128 has a very low offset voltage of 50 µV (max) with a drift of 0.5 V/°C (max) and a high common-mode rejection of 120 dB at G ≥ 100. The inputs are over-voltage protected up to ±40 V. It can operate at a very low voltage (as low as ±2.25 V) with a low quiescent current of 700 µA. The gain equation of INA128 is given as in Equation 4.7:

$$G = 1 + \frac{50K\Omega}{R_G} \tag{4.7}$$

where:

R_G is the gain resistor that decides the desired gain.

Figure 4.8 shows the schematic of connection between the electrical bridge and INA128p.

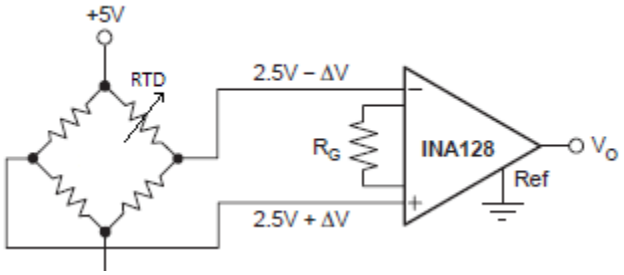

Figure 4.8 Schematic layout of the signal amplification circuit

4.6 Difference Circuit

The INA128 amplifier is used to design a differential circuit. The outputs from two Wheatstone bridge circuits are fed into the INA128 amplifier. Figure 4.9 shows the schematic of the difference circuit.

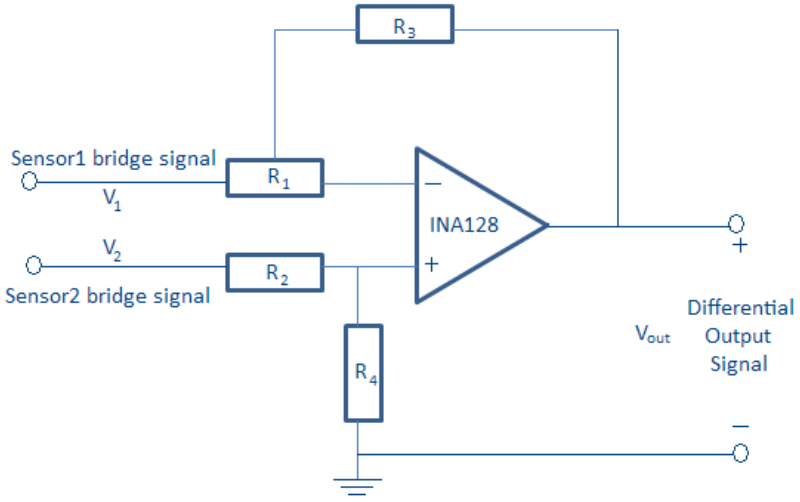

Figure 4.9 Schematic layout of the difference circuit

The differential output signal from the amplifier circuit is given as in Equation 4.8:

$$V_{out} = \frac{(R_3 + R_1)R_4}{(R_4 + R_2)R_1} V_2 - \frac{R_3}{R_1} V_1$$

(4.8)

The values of the resistors are chosen such that the gain of the difference is unity as shown in Equation 4.9 and the circuit output is simply the difference of the two input signals as shown Equation 4.10.

$$R_1 = R_3 \; and \; R_2 = R_4$$

(4.9)

$$V_{out} = V_2 - V_1$$

(4.10)

4.7 The Pulse Generator

A pulse generation circuit is designed in order to operate the heating element in a pulse mode. A timer IC (LM555) from National Instruments is used in the pulse generation circuit. The LM555 is small size 8-pin MDIP chip.

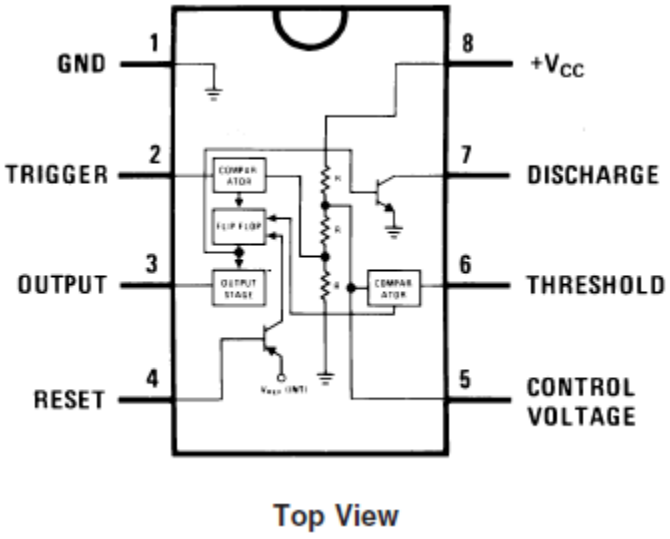

Figure 4.10 Pin layout of timer LM555 IC

The LM555 is a highly stable and can generate accurate time delays. The LM555 is operated in astable mode. In this mode the duty cycle/time delays are accurately controlled with two external resistors and one capacitor. Figure 4.11 shows the of the timer circuit for astable mode

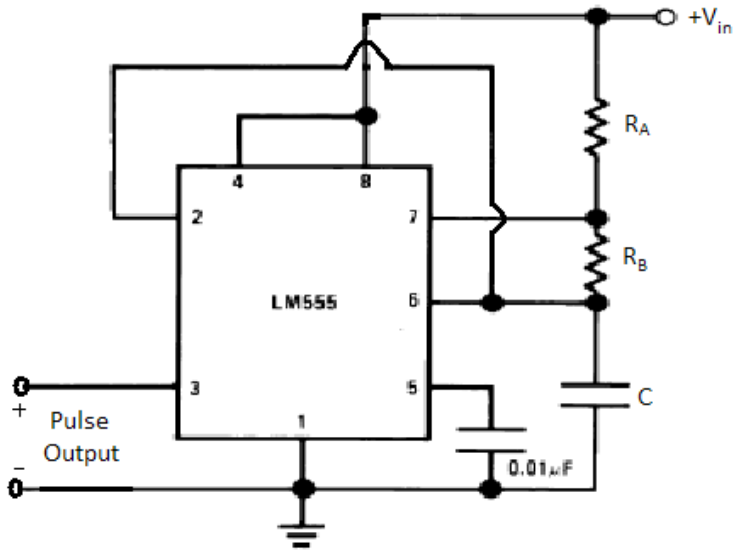

Figure 4.11 Schematic layout of the timer IC circuit in astable mode for pulse generation

In this circuit, when a DC input is supplied to the LM555 timer, the capacitor C charges through the resistors RA and RB. The capacitor charge eventually builds up enough voltage to trigger an internal comparator to toggle the output flip-flop. Once the flip-flop is toggled the capacitor C discharges through RB into the discharge pin (pin #7). When the capacitor C's voltage reaches the low limit, another internal comparator is triggered to toggle the output flip-flop. The capacitor C charges again and the cycle is repeated.

The high time of the pulse can be set using Equation 4.11:

$$t_{on} = 0.693(R_A + R_B) \cdot C \tag{4.11}$$

The low time of the pulse can be set using Equation 4.12:

$$t_{off} = 0.693(R_B) \cdot C \tag{4.12}$$

The total period can be given by Equation 4.13:

$$t = t_{on} + t_{off} = 0.693(R_A + 2R_B) \cdot C \tag{4.13}$$

4.8 Conclusion

The above described system allows portability and high level of integration. Based on the energy level of consumption various approaches may be followed. In this approach an energy level within 10 J/s may be appropriate. High energy power supplies may be utilized to provide higher energy levels for higher temperature distribution. The latter lacks flexibility and system portability.

5. EXPERIMENTAL SETUP

This Chapter discusses the in-lab arrangement of experimental assembly of the calorimetric thermal mass flow sensor. A computational fluid dynamic (CFD) simulation model replicating the boundary and subdomain conditions of the experimental setup was developed to predict the calorimeter response to air and water flow. The experimental results are presented and compared with the simulated predictions.

5.1 Experimental Assembly Model

To validate the proposed methodology to measure a streamline fluid flow, a thermal mass flow sensor was assembled using the available resources as shown in Figure 5.1. The construction of calorimeter is discussed below along with the electrical circuits and data acquisition scheme used to operate, sense, and record the signals from the sensing elements.

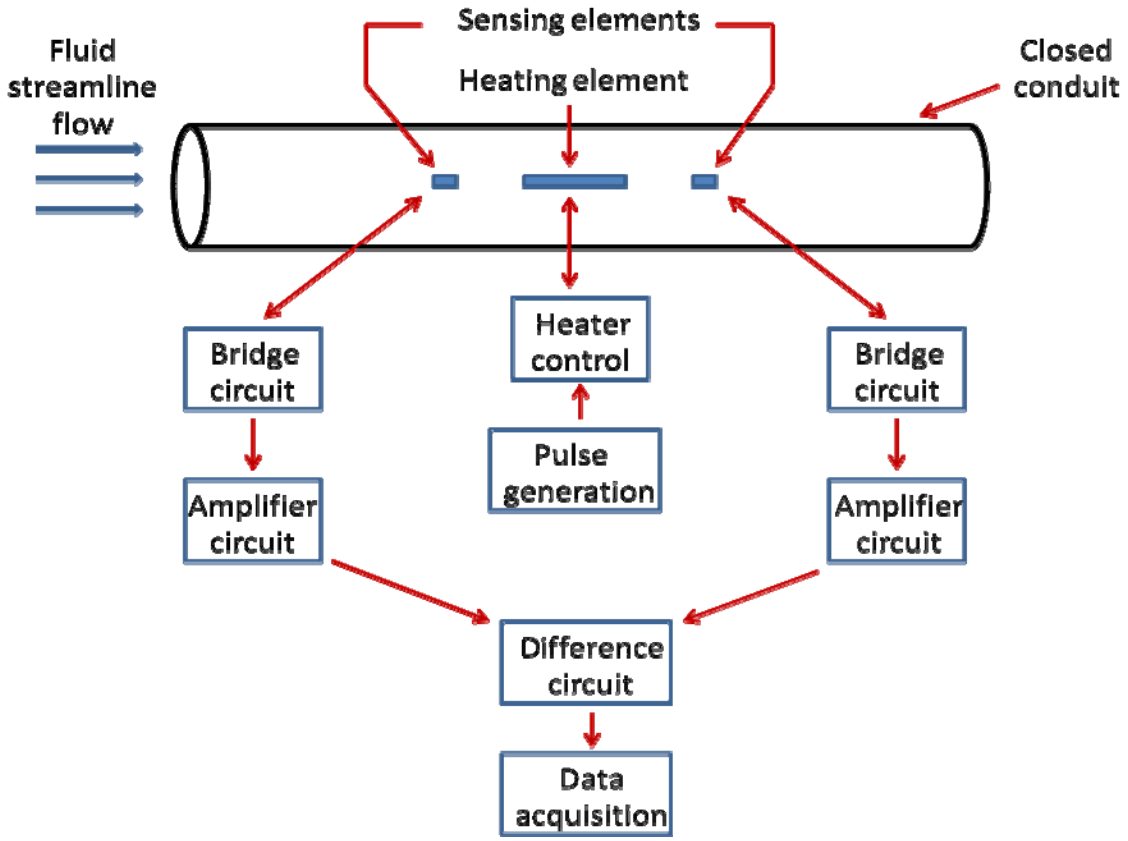

Figure 5.1 Flow measurement system layout

5.1.1 Calorimetric Mass Flow Meter Design

The overall approach for the calorimetric mass flow meter was based on prevalent industrial designs [5]. The experimental assembly of the sensor consisted of a thinfilm heating element positioned in the middle of two sensing elements. The heating element was the Polyimide Thermorfoil heater/Kapton heater, and the sensing elements were thinfilm Platinum RTDs as described in Chapter 4. Figure 5.2 shows the cross section of the PVC pipe used to encapsulate the sensor assembly. Holes of the size of the heating and sensing elements were drilled into the PVC pipe. After inserting the elements, the holes were sealed with 100% pure Silicone to provide thermal insulation.

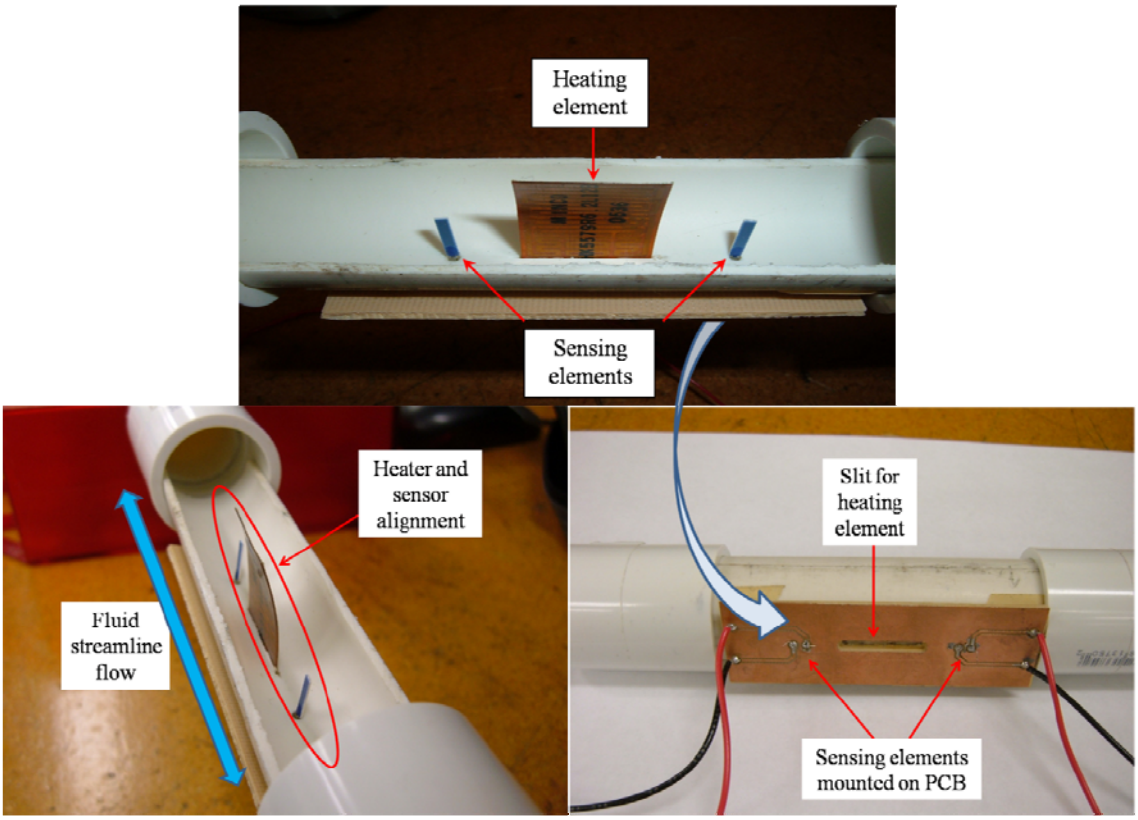

Figure 5.2 Experimentally assembled calorimetric thermal mass flow sensor

Figure 5.2 shows the placement and alignment of the heating and sensing elements. The sensing elements were placed 1 cm from the heating element edges in each direction, and were aligned with the edges of the heating element. Figure 5.2 shows the PCB used to mount the sensing elements.

5.1.2 Electrical Circuitry Design

With the help of the integrated analog circuits, the signal from the sensing elements was acquired. Each sensing element was connected to an individual electrically balanced Wheatstone bridge. The output voltage signal from each bridge circuit was fed to separate instrumentation amplifier ICs. Since the output signals from the bridge

circuits were in millivolts, the gain of the amplifiers was set to ~100 to get the sensor response in volts. The outputs from the amplifiers were fed to a difference circuit, which also consisted of an instrumentation amplifier IC with no gain. Figure 5.3 shows the schematic of the circuit that was used to acquire the signal from the sensing elements, further, the difference signal was logged into the computer using Agilent 34401A multimeter.

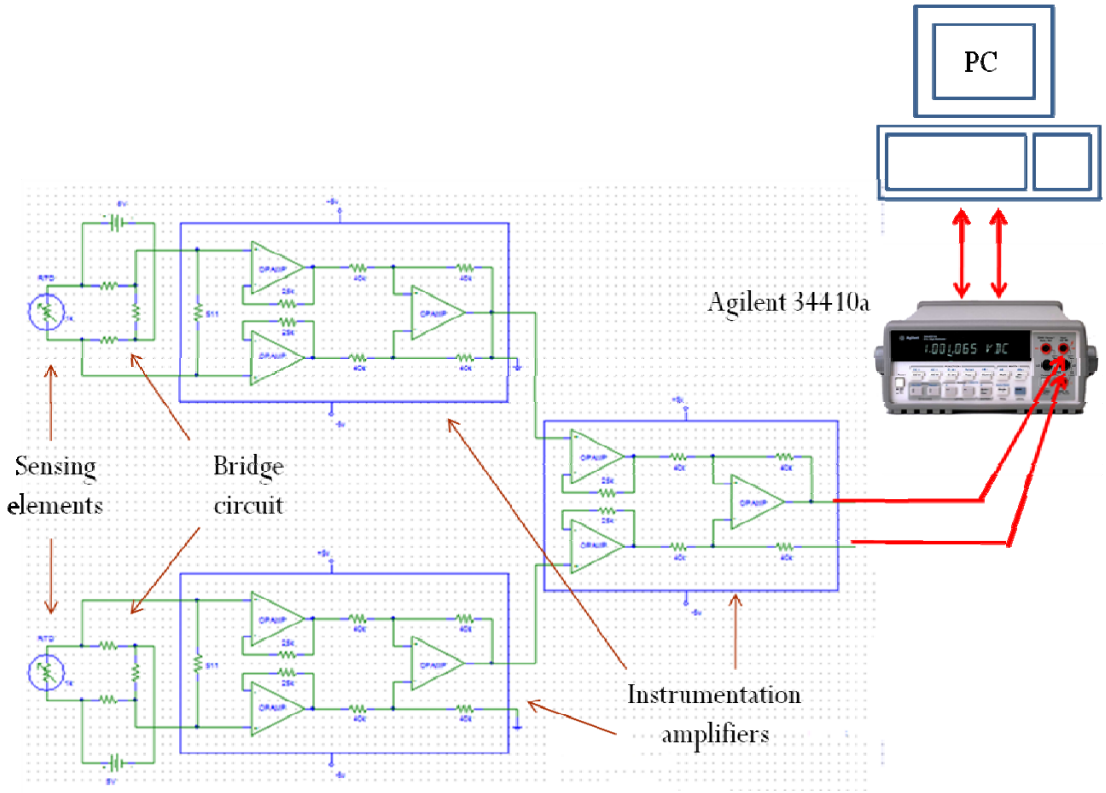

Figure 5.3 Schematic layout of the sensing circuit and data acquisition scheme

The heater temperature control was achieved using Minco temperature controller (CT325). The pin description of the controller unit was described is Chapter 4. The controller was set to maintain the heater at a constant temperature of 55 °C.

Figure 5.4 shows the controller arrangement with the RTD as part of the feedback control for keeping the heat at constant temperature.

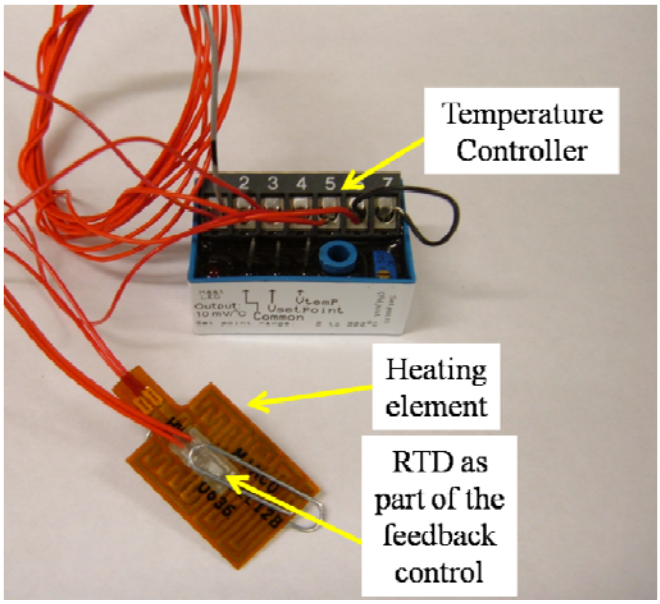

Figure 5.4 Heater temperature control scheme

The heating element was operated in pulse mode. The pulse generation was achieved using a timer (LM555) IC. The pins and configuration of LM555 is described in Chapter 4. The values of resistors and capacitors were selected such that the high time and low time of the pulse was 60 s each, i.e. 50% duty cycle. Figure 5.5 shows the schematic of LM555 connected with the temperature controller unit.

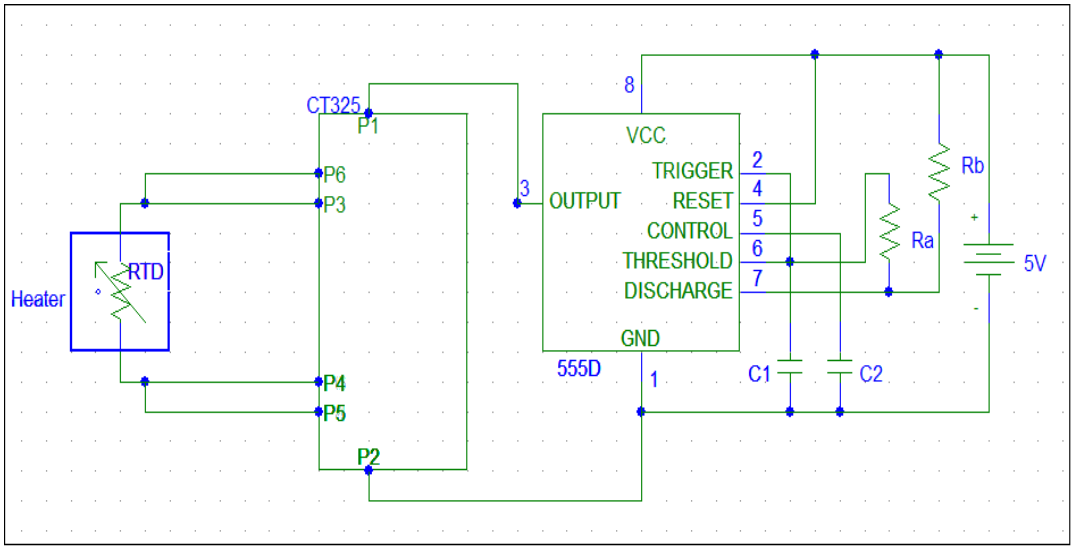

Figure 5.5 Schematic layout of the timer circuit/pulse generation

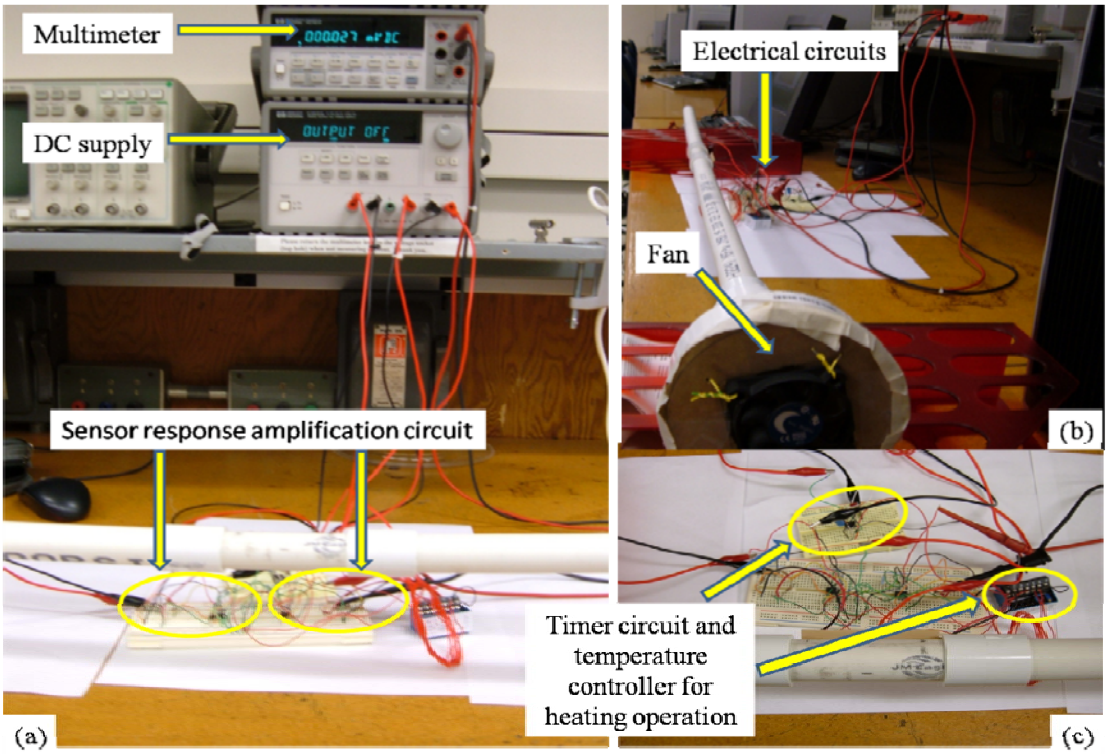

Figure 5.6 Experimentally setup of the assembled calorimetric thermal mass flow sensor

Figure 5.6 shows the in-lab experimental setup of the assembled thermal mass flow sensor. An off-the-shelf, 12V rated, CPU cooling fan was used to create an air flow. A wide range of air flow was achieved by varying the power supplied to the cooling fan. Table 5.1 shows the air flow achieved with respect to the voltage at which the cooling fan was operated. The flow measurement was done using an EXTECH Datalogging/Printing Anemometer (Model #451181).

Table 5.1 Flow rates with respect to fan operation voltages

Fan operation volatge (V)	Velocity (m/s)	Flow rate (L/m)
6	0.6	17.87846401
8	0.8	23.83795201
10	1	29.79744002
12	1.2	35.75692802

5.2 Computational Fluid Dynamics (CFD) Simulation

A CFD simulation of heat and mass flow in a calorimetric thermal mass flow sensor was performed with the help of COMSOL Multiphysics. The Navier-Stokes and heat conduction/convection equations that were simulated are stated in Section 3.2. The simulation of the sensor was performed for operation in air and water.

5.2.1 Model Geometry and Boundary Conditions

A geometric model replicating the actual size of the experimental assembly of the calorimetric thermal mass flow sensor was constructed in COMSOL. Figure 5.7 shows the geometric model of the sensor in COMSOL.

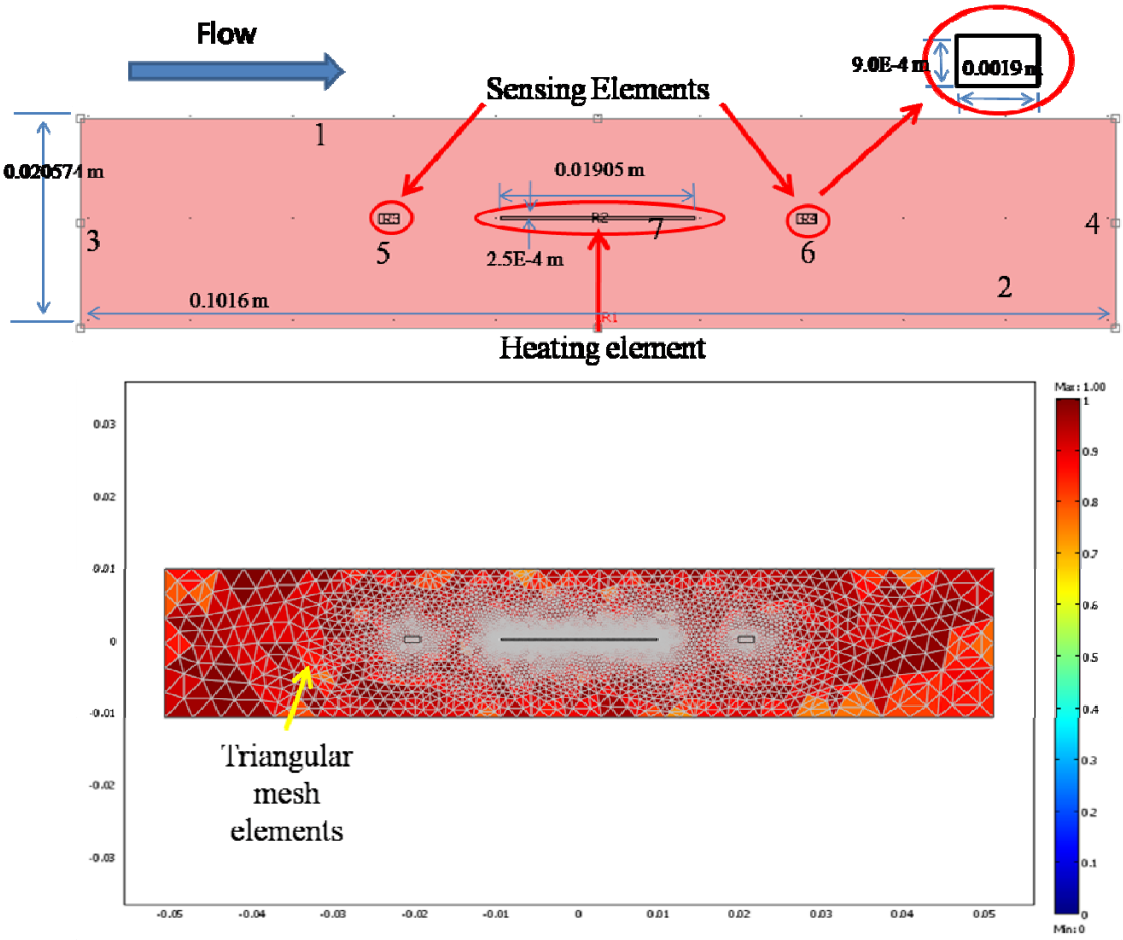

Figure 5.7 Sensor geometry and mesh elements in COMSOL

The geometric model was solved for incompressible Navier-Stokes, Conduction and Convection. Prior to solving the model, the geometry was meshed and refined to provide good quality elements near the heater and sensor surfaces. Figure 5.7 shows the triangular mesh elements and their quality, which is a scalar quantity. The measure is defined for each mesh element where 0 represents the lowest quality and 1 represents the highest quality. Table 5.2 gives the mesh statistics.

Table 5.2 Mesh statistics

Number of mesh points	5272
Number of triangular mesh elements	10436
Number of degrees of freedom	62929
Number of boundary elements	354
Number of vertex elements	16
Minimum element quality	0.7057
Element area ratio	7.45E-4

Once the meshing was complete, first the incompressible Navier-Stokes solution was generated using Lagrange stationary solver. Table 5.3 shows the subdomain and boundary conditions used to solve the model. A streamline artificial diffusion was selected for solving the Navier-Stokes (N-S) equations. After solving for x and y velocities, the N-S solutions were stored. The model was then solved for heat conduction and convection using a time-dependent solver. Time stepping was performed from 0 to 300 s with interval of 1 s. The relative and absolute tolerances of 0.01 and 0.001 were chosen, respectively. Table 5.4 shows the thermal subdomain and boundary conditions used to solve the problem. The pulse heating mode was made possible by using the inbuilt COMSOL Heaviside functions. Equation 5.1 shows the expression used to generate a square pulse for a period of 120 seconds with 50% duty cycle.

$$T = T_0 + T_a * \big(flc2hs(tm - 60{,}1) - flc2hs(tm - 120{,}1)\big)\, for\ t_m = (t, 120) \tag{5.1}$$

where:

T is the desired heating element temperature

T_0 is the initial temperature of the heating element

T_a is the desired temperature rise of the heating element from its initial value

t_m is the modulo operator

t is the time in seconds

$flc2hs(\ \ )$ is a smoothed Heaviside functions

Isotropic diffusion was enabled while solving the heat conduction and convection equations. Referring to Figure 5.7 for a flow from left to right, the temperature was recorded at the point, 0.01 meters, downstream and upstream from the respective edge of the heating element. The results for both air and water are shown in Section 5.2.2. Table 5.3 and Table 5.4 give the subdomain and boundary conditions selected for the simulation with air and water.

Case 1: Air

Table 5.3 Subdomain and boundary conditions for air

	Subdomain Conditions		**Boundary Conditions**	
Incompressible Navier-Stokes	Density (kg/m^3)	ρ = 1.184	1, 2, 5, 6 & 7	No slip
	Dynamic viscosity (Pa.s)	η = 18.1034E-6	3	Inflow/Outflow velocity
			4	Normal flow pressure
	Subdomain Conditions		**Boundary Conditions**	
Conduction and Convection	Thermal conductivity (W/(m.K))	k = 0.026	1, 2, 5, & 6	Thermal insulation
	Density(kg/m^3)	ρ = 1.184	3	T = 298 °K
	Heat capacity (J/(kg.K))	Cp = 1005.38	7	Desired heater Temp. in °K
			4	Convective flux

Case 2: Water

Table 5.4 Subdomain and boundary conditions for water

	Subdomain Conditions		**Bondary Conditions**	
Incompressible Navier-Stokes	Density (kg/m^3)	ρ = 998.2	1, 2, 5, 6 & 7	No slip
	Dynamic viscosity (Pa.s)	η = 1.0E-3	3	Inflow/Outflow velocity
			4	Normal flow pressure
	Subdomain Conditions		**Bondary Conditions**	
Conduction and Convection	Thermal conductivity (W/(m.K))	k = 0.0015 * T + 0.1689	1, 2, 5, & 6	Thermal insulation
	Density(kg/m^3)	ρ = 998.2	3	T=298 °K
	Heat capacity (J/(kg.K))	Cp = 4200	7	Desired heater Temp. in °K
			4	Convective flux

5.2.2 Simulation Results

Figure 5.8 shows the average of peak temperature difference between the upstream and downstream sensing element at different air flow rates. The heating element was operated in pulse mode with 50% duty cycle with peak temperatures at 30 °C, 35 °C, 40 °C, 50 °C and 55 °C. We find that the temperature difference decreases as a function of flow rate. This is intuitive because the downstream sensing element, which gets heated by the convective heat transfer from the heating element, also cools off much faster if the flow of air is higher. The simulations show that using a higher heater temperature gives a higher slope and hence higher sensitivity in flow measurements. We also find that by increasing the heater temperature, a dynamic range of flow can be measured. The increase in flow range with heater temperature can be observed in the area marked by the red lines.

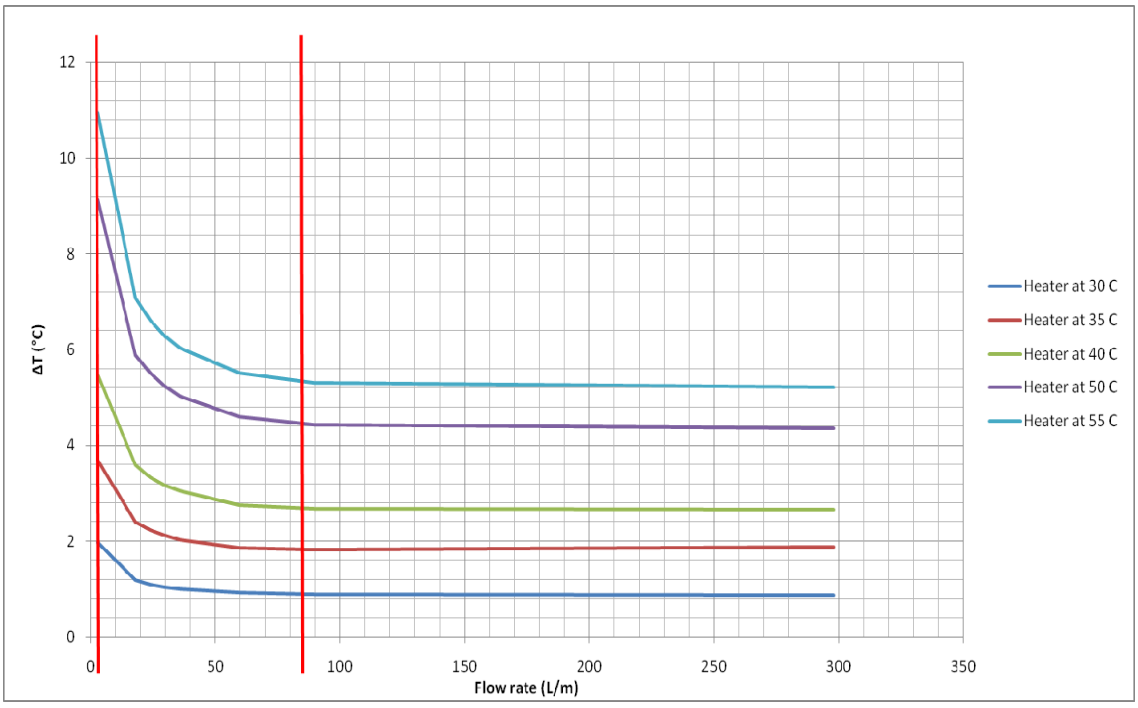

Figure 5.8 Peak temperature difference versus air flow rate

Figure 5.9 shows the average of peak temperature difference between the upstream and downstream sensing element at different water flow rates. The heating element was operated in pulse mode with 50% duty cycle with peak temperatures at 40 °C, 60 °C, 80 °C. Observation for flow sensing in water was found to be similar as in air. The temperature difference was found to decrease with the increase in water flow rate, and having a higher heater temperature increased the sensitivity (slope) for flow sensing. Since water has a higher kinematic viscosity, water sensing had to be simulated at lower flow rates in order to remain the laminar flow regime (Re <500 in simulations). We also find that by increasing the heater temperature, a dynamic range of flow can be measured. The increase in flow range with heater temperature can be observed in the area marked by the red lines.

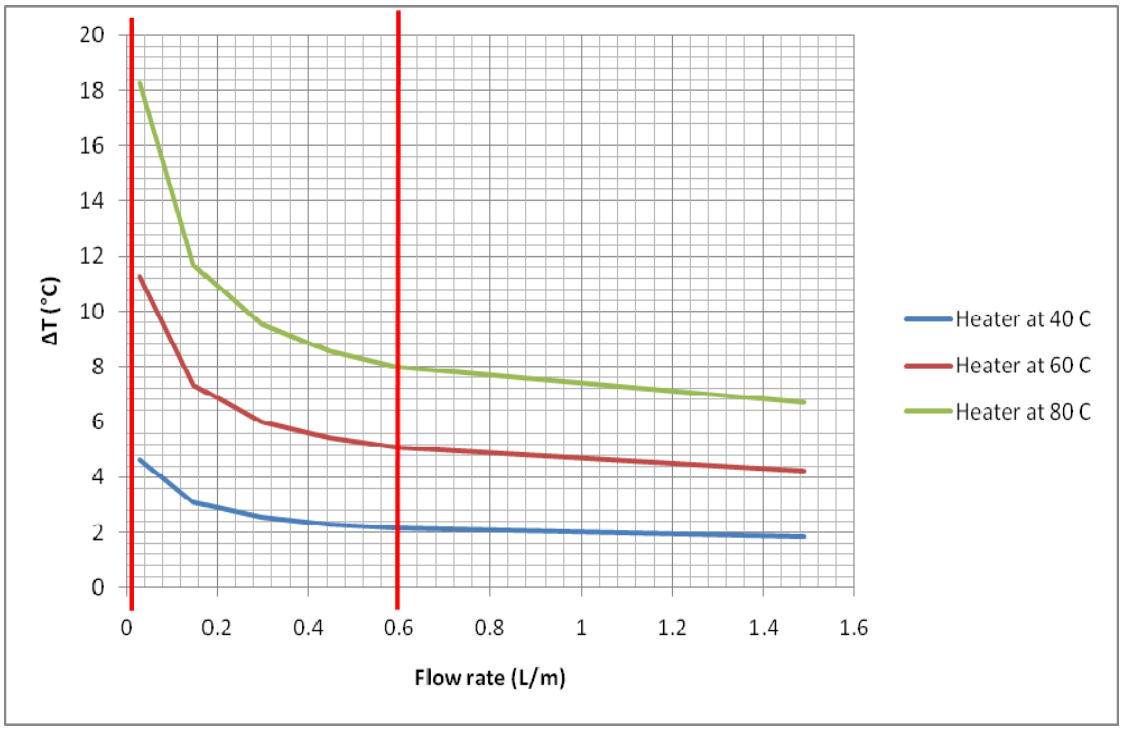

Figure 5.9 Peak temperature difference vs. water flow rate

5.3 Experimental Results

Figure 5.10 shows the plot of the temperature difference between the upstream and downstream sensing elements with respect to time. The heating element was operated in pulse mode and the heat pulse peak was set to 55 °C. The high and low time for the pulse were 60 seconds each, i.e. 50 % duty cycle. On observing the graph, it can be seen that with the increase in the flow rate the differential temperature between the sensing elements decreases. The negative difference is due to the flow in the opposite direction.

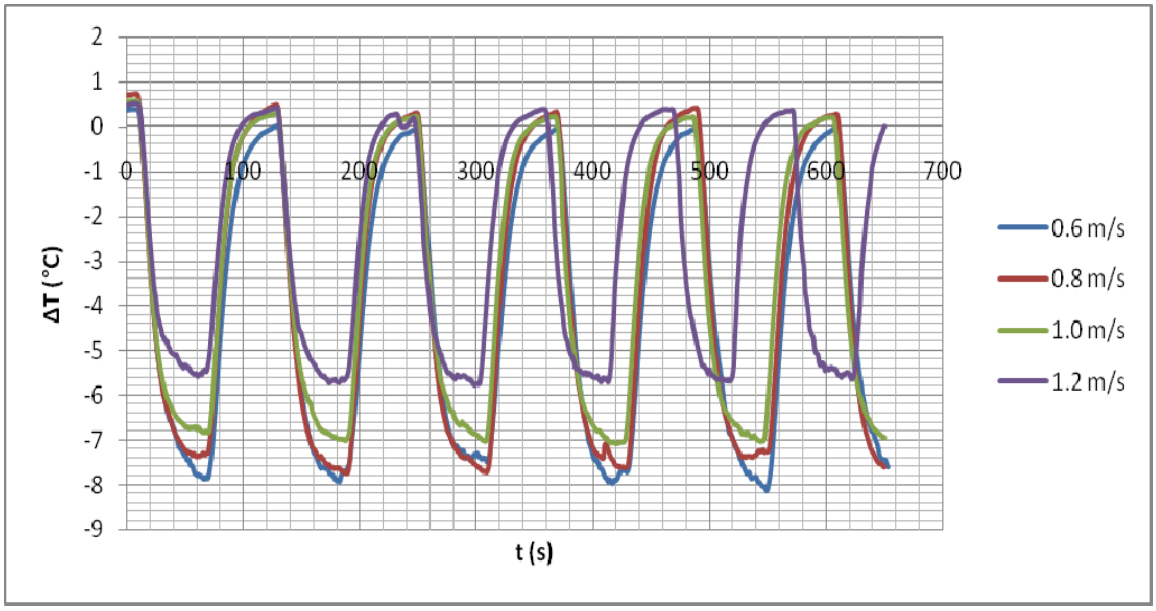

Figure 5.10 Plot of temperature difference between upstream and downstream vs. time

Figure 5.11 shows the average of peak temperature difference between the upstream and downstream sensing element at different air flow rates. The heating element was operated in pulse mode with 50% duty cycle at 35 °C and 55 °C. As predicted from the simulation, we see the temperature difference decreases as velocity increases. At 35 °C, the simulation and experimental results show close resemblance. However, at 55 °C, the simulation and experimental results vary in nature. This can be

explained by the fact that the heat losses increase as the heater temperature increases. To avoid this difference, the experimental setup needs better heat modeling.

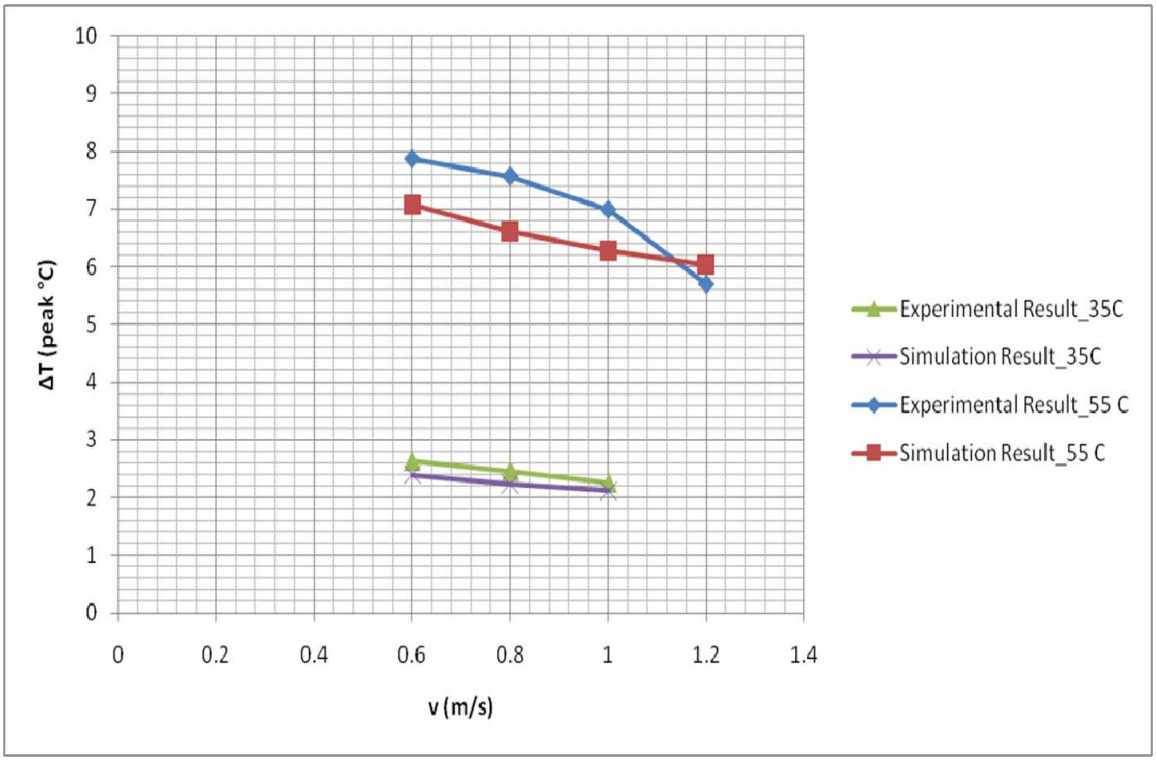

Figure 5.11 Experimental result and simulated result comparison

We also tried to measure the cooling rate of the sensing element as a function of the air flow rate, since it could potentially be used to infer air flow rate directly. Figure 5.12 shows the differential cool-off rate of the downstream sensing element. The heating element was operated in pulse mode with 50% duty cycle at temperatures 40 °C, 50 °C and 55 °C. Data shows that with increase in the flow rate the cool-off rate also increases. Better linearity is seen with higher heater temperatures. This promises that cool-off rate of the downstream sensing element may also be used to infer or confirm the air velocity.

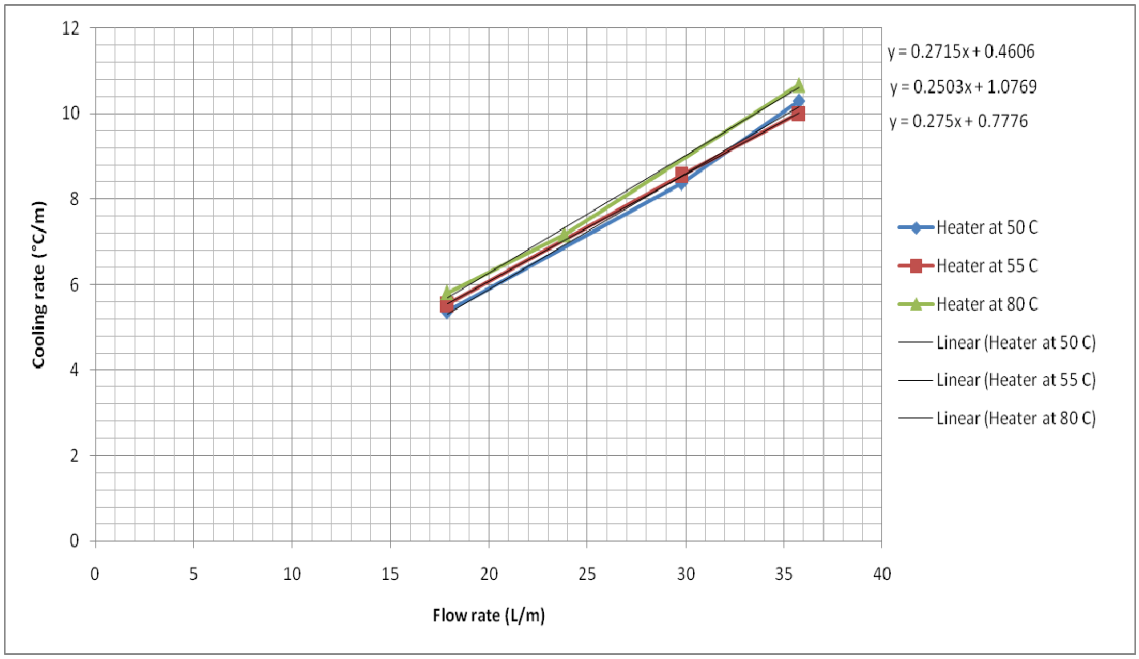

Figure 5.12 Cool-off rate as a function of air flow rate

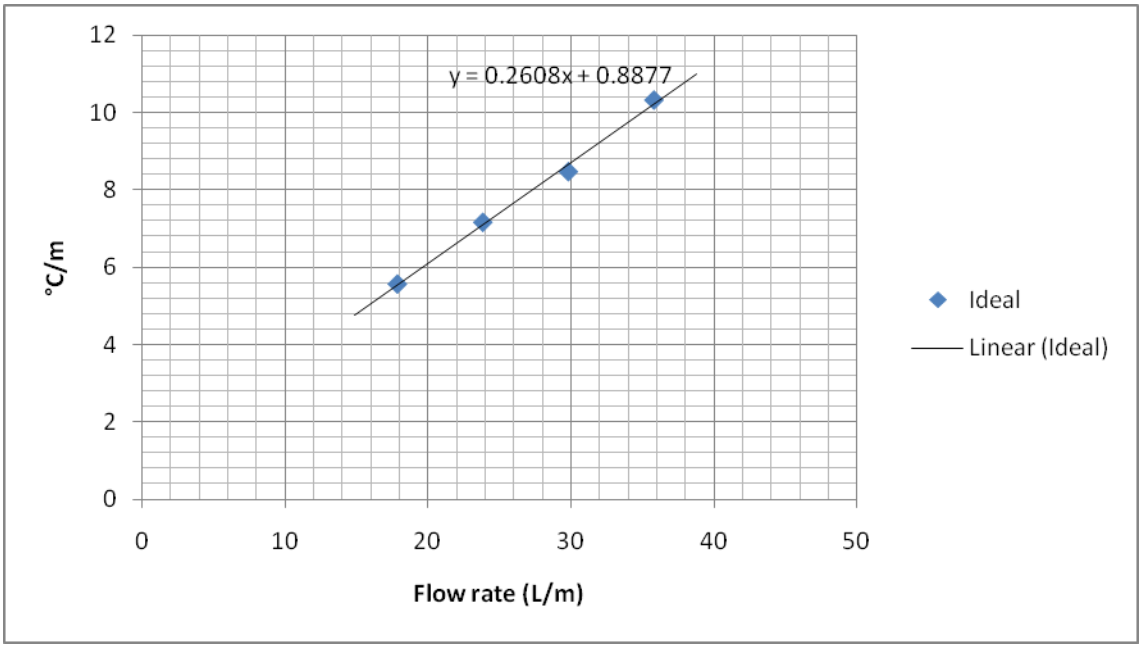

Figure 5.13 The average plot of the cool-off rates as a function of air flow rate

Figure 5.13 shows average of the cool-off rates measured using the experimental setup operated at different heater temperatures. From the graph, we see that the overall relationship between the cool-off rate and the flow rate is linear. This linearity can help infer the air flow rates directly for a measured cool-off rate.

Figure 5.14 is the plot of the differential temperature of the upstream and downstream sensing elements versus the time. The figure also shows the feasibility to sense the bi-directional flows using the experimentally assembled calorimetric mass flow sensor.

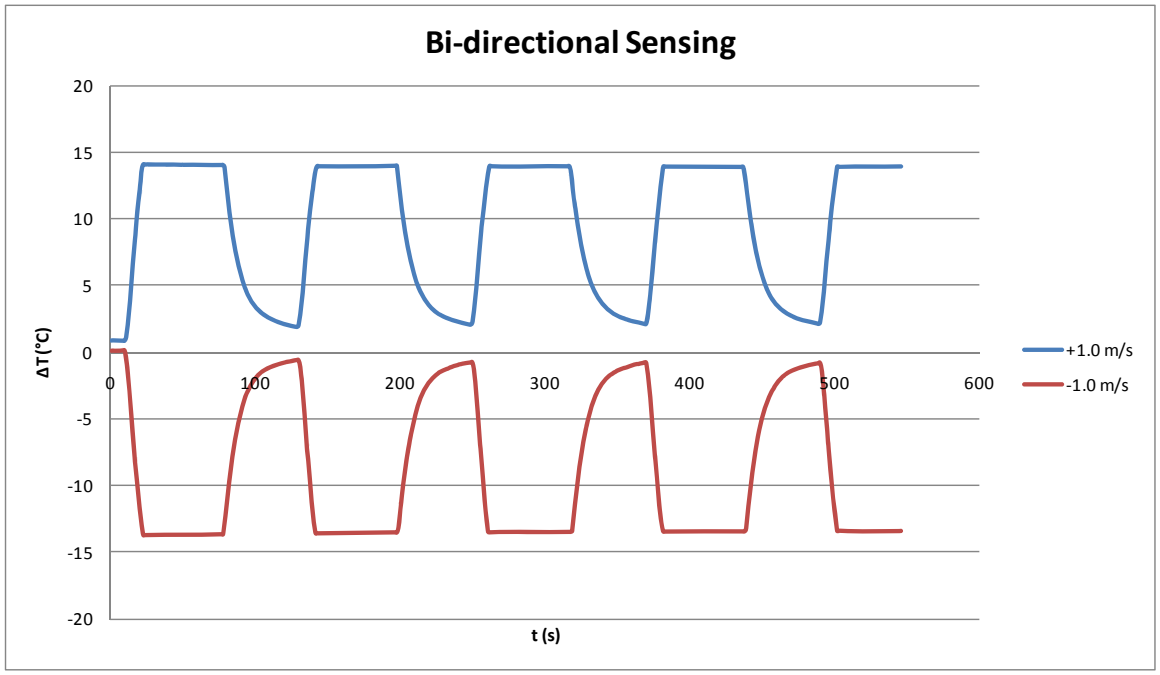

Figure 5.14 Bi-directional sensing feasibility

Figure 5.14 shows the plot of differential temperature of the upstream and downstream sensing elements with respect to time at various flow rates. The negative difference is due to the flow in the opposite direction. In this case the heating element is operated in pulse mode at a higher temperature in order to get the sensing elements to reach their equilibrium state. Figure (a) shows the result plot with the heating element operated in pulse mode with 50% duty cycle. Figure (b) shows the result plot with the heating element operated in pulse mode with 25% duty cycle. It can be observed that with the reduction in the duty cycle the results remain unaffected. The energy consumption requirements shown for the continuous heating, 50% duty cycle heating, and 25% duty cycle heating show that the sensor would consume less power while providing similar flow rate sensitivity as 50% or 100% duty cycle operation.

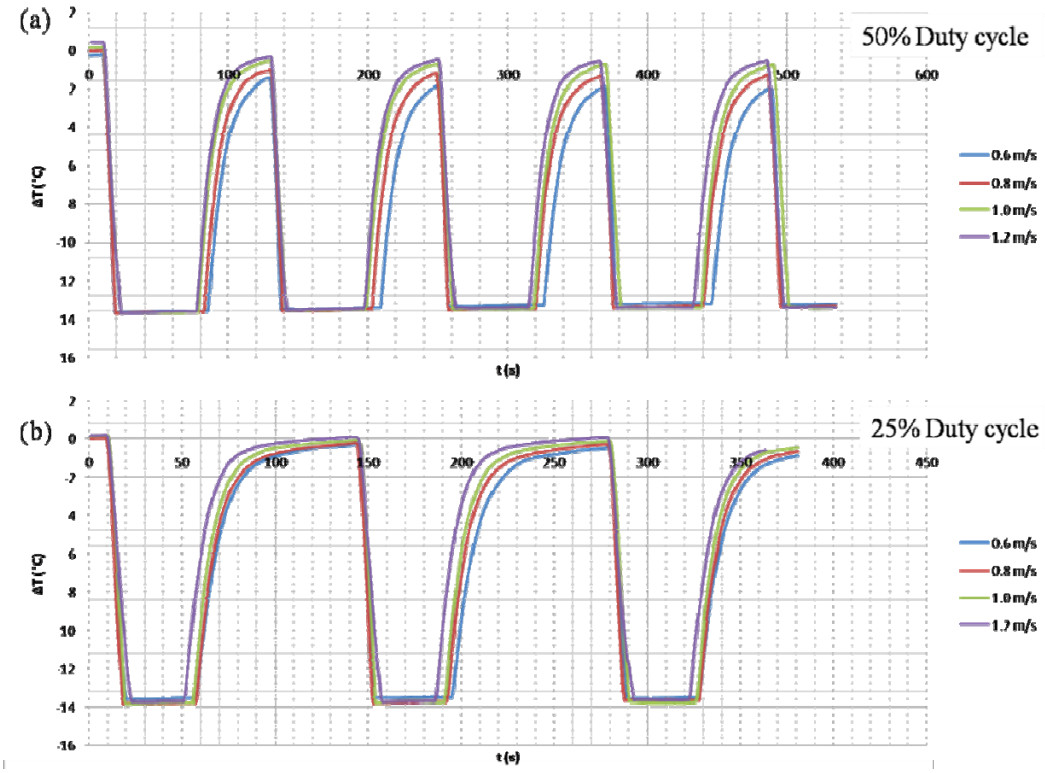

Figure 5.15 (a) The heating element operated in pulse mode with 50% duty cycle, and (b) The heating element operated in pulse mode with 25% duty cycle.

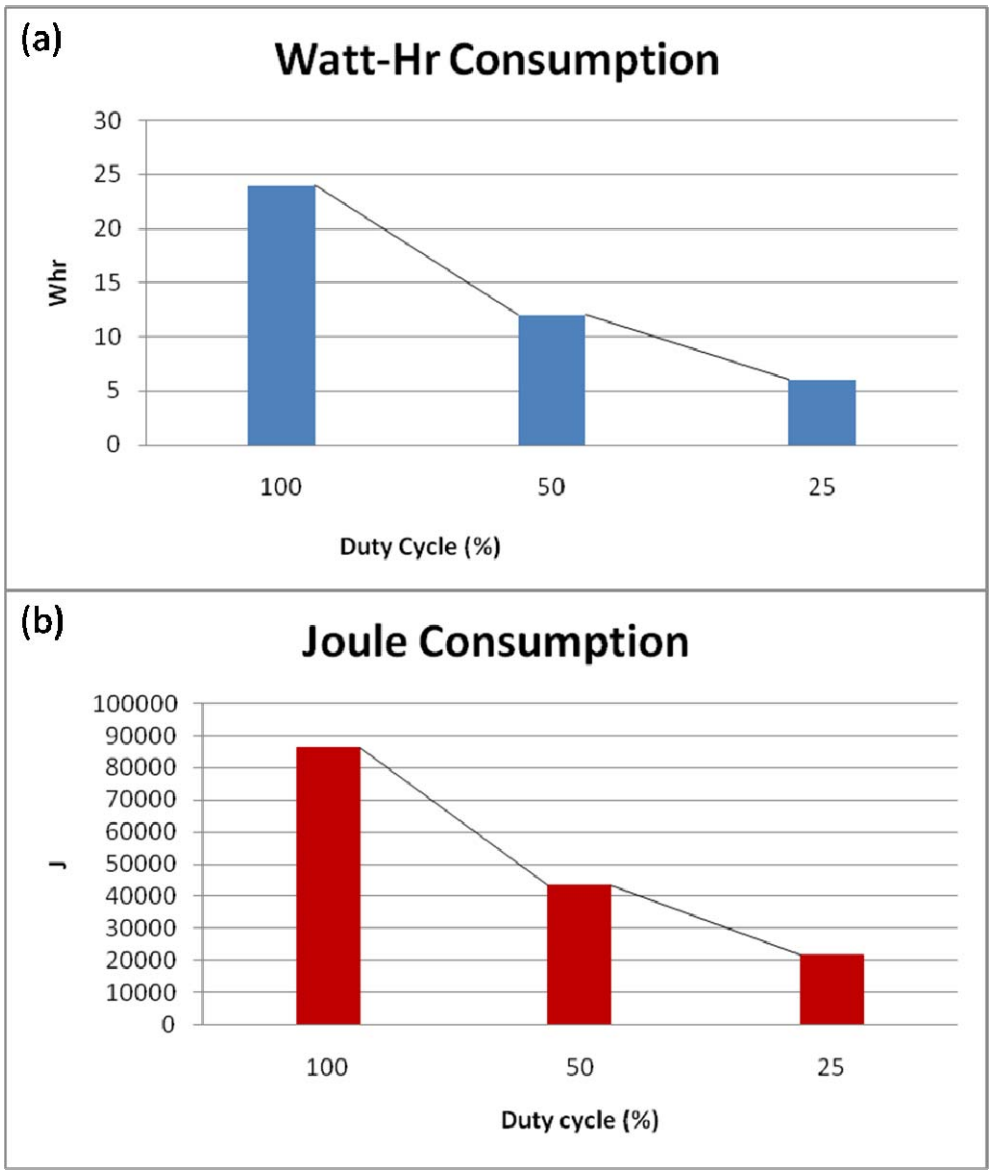

Figure 5.16 (a) Watt-hour consumption and (b) Joule consumption

Figure 5.15 show the energy consumption of the heating operation in the experimentally built thermal mass flow sensor. This graph shows how reducing the duty cycle of the heat pulse the energy consumption also can be reduced.

6. CONCLUSION AND FUTURE WORK

In this research project, a calorimetric thermal mass flow sensor was experimentally assembled and tested to measure flow rates in a closed conduit. Air and water flow were simulated using COMSOL software. The simulations were based on a mathematical model that was required to solve the Navier-Stokes fluid flow equations and the heat conduction/convection equation with boundary settings reflecting near-real situation. The air flow model was validated experimentally with flow range between 0.6 to 1.2 m/s.

In this work we have demonstrated the design of thermal sensor using thinfilm platinum sensor and polyimide thermofoil heating element. This provided the thermal responses expected for the design. The low power instrumentation amplifier provided very accurate measurements, and as low as ~2.5 μV (50 μV max) change was detected. This corresponds to a temperature change as low as 0.02 °C. The difference amplifier provided the direction of the flow. The selection of the temperature controller provided a very stable and accurate temperature distribution in the vicinity of the sensor. The timer circuit was designed to carry out heating operation in pulse mode with 25% and 50% duty cycle.

A computational fluid dynamic (CFD) model replicating the boundary conditions of the assembled flow sensor was built using COMSOL Multiphysics. Simulations for air and water flows were performed. The experimental results were in close agreement with the simulation results.

The experimental results showed that a dynamic flow measurement range can be achieved by increasing the heater temperature. From the results, it was clear that by reducing the duty cycles the power consumption of the system can be reduced without having any adverse effects on the flow sensitivity of the sensor. It was also concluded that the cool-off rate of the sensors can be a potential measure to predict the flow rate of the fluid under measurement. The challenges in experimental verification of the liquid flow included control of flow and electrical isolation of the sensing elements within the liquid medium. An epoxy material has been identified that can be possibly used for isolation. This was reserved for future consideration. In future we would like to realize a system that can be integrated with wireless devices that can transmit the magnitude of the fluid flow and its direction.

LIST OF REFERENCES

LIST OF REFERENCES

[1] F. Mayer and M. Lechner, "Method and Sensor For Measuring a Mass Flow," U.S. Patent 6,550,324, April 22, 2003.

[2] J. Olin, "The Evolution of Thermal Mass Flow Meters," October 2002, http://sierrainstruments.com/prnews/a6.pdf.; Last accessed March 2010.

[3] P. Bradshaw, "Thermal methods of flow measurement," *Journal of Physics E: Scientific Instruments*, vol. 1, 1968, pp. 504-509.

[4] Z. Tan, M. Shikida, M. Hirota, and K. Sato, "On-wall in-tube inserted thermal flexible micro sensors for measuring mass-flow," *IEEE International Symposium on Micro-NanoMechatronics and Human Science, 2005*, pp. 238-243.

[5] B. Zimmerman, "Appliance sensors become hot stuff," *Machine Design, pp. S14-S18*, May 2005.

[6] A. Bauer, "Direct measurement of velocity by hot-wire anemometry," *AIAA*, vol. J.3, 1965, pp. 1189-1191.

[7] P. Handford and P. Bradshaw, "The Pulsed-Wire Anemometer," *Experiments in Fluids*, vol. 132, 1989, pp. 125-132.

[8] A.B. Boyd, "Mass flow meter," U.S. Patent 4,335,605, May 14, 1980.

[9] "Sierra Flow Meters," http://www.sierrainstruments.com/; Last accessed June 2009.

[10] "Omega Flow Meters," http://www.omega.com/prodinfo/flowmeters.html; Last accessed June 2009.

[11] "ABB Flow Measurement Products," http://www.abb.com/product/us/9aac100398.aspx?country=US; Last accessed June 2009.

[12] J.G. Webster, R. Thorn, Z.D. Husain, D.J. Wass, N. Nguyen, and J. Webster, *The Measurement, Instrumentation, and Sensors Handbook*, CRC Press LLC, 1999.

[13] W. Hennessy, "A Review of Your Flow Sensing Options," October 2006, http://www.sensorsmag.com/sensors/flow/a-review-your-flow-sensing-options-1209; Last accessed November 2009.

[14] "Types of Flow Meters," 2005, http://www.engineeringtoolbox.com/flow-meters-d_493.html; Last accessed February 2010.

[15] "Flowmeter: Positive Displacement," 2002, http://www.smartmeasurement.com/en/documents/flowmeter/positivedisplacement.asp; Last accessed February 2010.

[16] "Mass Flows," http://www.massflows.com/; Last accessed March 2010.

[17] M.C. Elwenspoek, "*Thermal flow micro sensor," 1999.* In: Proceedings of the 1999 International Semiconductor Conference (CAS '99), 05-09 Oct 1999, Sinaia, Romania. pp. 423-435. IEEE Computer Society Press. ISBN 0-7803-5139-8.

[18] S. Beeby, *MEMS mechanical sensors*, Artech House, Inc., MA, 2004, pp. 217-225.

[19] R. Yadav, *Heat and Mass Transfer*, Central Publishing House, Allahabad, 1997.

[20] F. Incropera and D. DeWitt, *Introduction to Heat Transfer*, John Wiley and Sons, NJ, 1985.